Phase Decomposition and Magnetic Properties of Spinel Ferrites Synthesized via High-energy Ball Mill

by

Yiwen Wang

Bachelor of Science, Xi'an Jiaotong University, 2019

Submitted to the Graduate Faculty of the

Swanson School of Engineering in partial fulfillment

of the requirements for the degree of

Master of Science in Materials Science and Engineering

University of Pittsburgh
2021

UNIVERSITY OF PITTSBURGH

SWANSON SCHOOL OF ENGINEERING

This thesis was presented

by

Yiwen Wang

It was defended on

March 31, 2021

and approved by

Paul Ohodnicki, Ph.D., Associated Professor, Department of Mechanical Engineering and
Materials Science

Ahmed Talaat, Ph.D., Department of Mechanical Engineering and Materials Science

Thesis Advisor: Jung-Kun Lee, Ph.D., Professor, Department of Mechanical Engineering and
Materials Science

Phase Decomposition and Magnetic Properties of Spinel Ferrites Synthesized via

High-energy Ball Mill

Yiwen Wang, M.S.

University of Pittsburgh, 2021

Thermodynamically-induced phase separation which has been reported in several metal systems have huge influences on magnetic and structural properties. In comparison to metal systems, there has been limited research on the phase separation behavior of ceramics. In this study, cobalt spinel ferrite powders $Co_xFe_{3-x}O_4$ that is known to exhibit spinodal de composition was prepared via high-energy planetary ball mill to examine the potential of exploiting the spontaneous phase separation to control the magnetic properties of bulk ceramics. To study how high-energy ball mill and different conditions during process influence the phase separation behavior and properties, especially magnetic properties, of spinel ferrite powders, we produced and sorted several groups of $Co_xFe_{3-x}O_4$ powders with different nominal composition, milling time, calcination temperature, and subsequent thermal annealing temperature/time. VSM test result at room temperature (300K) and XRD analysis show that $Co_xFe_{3-x}O_4$ powders near the boundary of spinodal decomposition regime and at the center of the spinodal decomposition regime experience a different phase separation behavior. This difference is accompanied by a change in the magnetic properties (e.g. saturation magnetization and coercive field). A relation between the phase separation and the magnetic properties is explained from the viewpoint of the co-existence of multiple magnetic phases.

Table of Contents

List of Tables

List of Figures

1.0 Background and Literature Review

Magnetic material is a kind of functional material with a long history and a wide range of uses, which is closely related to informatization, automation, national defense, national economy and many other aspects. Among them, spinel ferrite materials are widely used and have great application value in various fields. The research on its preparation and magnetic properties has become one of the research hotspots. At the same time, the requirements on its performance are also increasingly high, and these properties largely depend on the preparation process.

With the development of industry and technology, the demand for high performance magnetic materials is increasing, especially under the condition of high work frequency. Some technologies like power generation and conversion required by not only enormous systems, but also some smaller systems, such as mobile communication platforms and components, are shifting to higher operation frequency. One of the most hot area at present, 5G communications, is in desperate need of the evolution of these technologies towards ultrahigh frequencies.

Scientific studies by materials researchers have been continuously directed toward developing the performance and properties of such materials. The goals are mainly about improving efficiency, reducing weight and cost in electronic devices, and reduce core loss (particularly eddy current loss at high frequency), and so on. There is no doubt that the synthesis, like mechanical alloying(MA), and processing, like spinodal decomposition(SD), are important steps to achieve the goals and many researchers have also applied a number of special techniques over the years that are being used to improve the property and performance of soft magnetic composites. In the future, the development and research will strengthen the combination of research, production and application, and constantly open up new application fields.

In this chapter, spinel ferrites especially cobalt ferrites, synthesis methods, processing and analysis tools will be involved.

1.1 Spinel Ferrites

Spinel ferrites are materials with a general chemical formula of AB_2O_4, where A and B are metallic cations positioned at two different crystallographic sites, which are called tetrahedral (A sites) and octahedral (B sites), composed of Fe as one of the main elements in such structure.

At present, magnetic oxides play an important role in many areas, like electronics industry and power applications. For each specific application, different material parameters play a role. Intrinsic parameters are different form those that are related to the microstructure. The intrinsic parameters such as the saturation magnetization, the magnetic anisotropy and the electrical conductivity, highly depend on the chemical composition, the electronic structure of the magnetic ions and the crystal symmetry in the lattice. Some important quantities for technical applications, such as permeability, coercive force or losses, depend strongly on grain size, porosity and inclusions, in other words, on the microstructure of the product. Therefore a combined effort of various scientific and technical disciplines is required to improve the performance.

Nowadays the design of many devices is considered to be satisfactory, although it is not totally ideal. Many efforts are made to improve the material properties, for instance, by looking at the periodic system in order to hit upon useful chemical additions or by changes in firing

techniques to improve the microstructure. However only very limited improvements can be achieved. More essential improvements are obtained by advances in technology, such as the use of very pure raw materials, or taking advantages of wet-chemical preparation methods. Microwave materials with unique properties have been obtained by relatively novel processing techniques such as hot-pressing.

Apparently superior properties, in other word, great parameters, means a lot. In order to make ideal products, fundamental research is required to control the various material parameters, related to their application. For instance, It is necessary to study exchange interactions to control the temperature dependence of the saturation magnetization. And when it comes to ceramics materials, the fundamental study of sintering processes and grain growth phenomena is of vital importance, which can lead to control of microstructure.
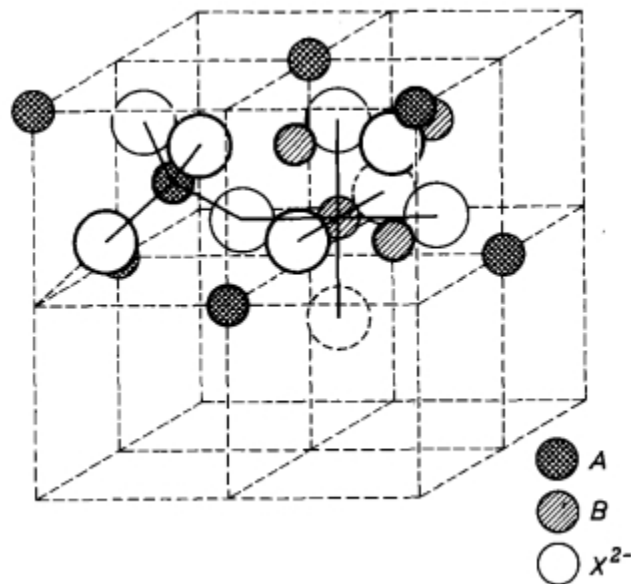
Fig. 1 Two octants of the unit cell of the spinel structure. A ions are on tetrahedral sites and B ions on octahedral sites of the X^{2-} anion packing. [1]

To achieve rational utilization and improvement of spinel ferrites, their structure should be learned at first. Compounds with the cubic spinel structure have the general composition AB_2X_4. The anions X, in most cases O^{2-}, form a cubic close-packed lattice. The A ions fill tetrahedral interstices and the B ions octahedral interstices of the anion packing. **Figure 1** shows two units AB_2O_4 in a quarter of the unit cell. In a tetrahedral site, like A ions in **Figure 1**, the interstitial is in the center of a tetrahedra forms by four lattice atoms. Three atoms, touching each other, are in plane; the fourth atom sits in the symmetrical position on top. Differently, an octahedral position for an (interstitial) atom is the space in the interstices between 6 regular atoms that form an octahedra, as B ions shown in **Figure 1**. Four regular atoms are positioned in a plane, the other two are in a symmetrical position just above or below. All spheres can be considered to be hard and touching each other. The six spheres define a regular octahedra, in its interior there is a defined space for an interstitial atom, bordered by six spheres.

The valency of the cations in spinels can range from monovalent to hexavalent and the most important magnetic ferrites are based on the composition $Me^{2+}Fe_2^{3+}O_4$, which is also our focus. This kind of spinel structure, which can also be called 2-3 spinels, can either have a "normal" structure or an "inverse" structure. In a normal structure, the divalent ions are on tetrahedral sites, the composition can be noted as $Me^{2+}[Fe_2^{3+}]O_4$ (the ions at the octahedrally coordinated B sites are placed between brackets, in this case, Fe_2^{3+}), and in an inverse structure, the composition can be noted as $Fe^{3+}[MeFe^{3+}]O_4$, in which the divalent ions are on octahedral sites. Zinc ferrite, and some metallic oxide like cobalt oxide are normal spinels, whereas nickel ferrite, $Fe[NiFe]O_4$, and Fe_3O_4 are common inverse spinels.

It is obvious that distribution of the cation will influence spinel structure, and the importance of the distribution of the cations over A and B sites for the magnetic properties can be clearly revealed in Fe_3O_4, a representative inverse spinel. Fe_3O_4 contains both Fe^{2+} and Fe^{3+}, so it often be viewed as a combination of $FeO \cdot Fe_2O_3$, or we can rewrite as $FeFe_2O_4$, which is, clearly, a spinel structure. Fe_3O_4 has a cubic inverse spinel group structure which consists of a cubic close packed array of oxide ions where all of the Fe^{2+} ions (A) occupy half of the octahedral sites and the Fe^{3+} (B) are split evenly across the remaining octahedral sites and the tetrahedral sites. Both FeO and γ-Fe_2O_3 have a similar cubic close packed array of oxide ions and this accounts for the ready interchangeability between the three compounds on oxidation and reduction as these reactions entail a relatively small change to the overall structure. The ferrimagnetism of Fe_3O_4 arises because the electron spins of the Fe^{2+} and Fe^{3+} ions in the octahedral sites are coupled and the spins of the Fe^{3+} ions in the tetrahedral sites are coupled but anti-parallel to the former. The net effect is that the magnetic contributions of both sets are not balanced and there is a permanent magnetism. To further understand how distribution of the cations affects other spinel ferrites, we can look at the differences between $ZnFe_2O_4$ and $MgFe_2O_4$ [1]. Both zinc ferrites and magnesium ferrites contain Fe^{3+} and a non-magnetic divalent ion, Zn^{2+} or Mg^{2+}. $ZnFe_2O_4$ has no spontaneous magnetization at room temperature, and when temperature goes below 9 K it shows antiferromagnetism. On the other hand, $MgFe_2O_4$ with cation distribution $Fe_{0.9}Mg_{0.1}[Fe_{1.1}Mg_{0.9}]O_4$ is ferrimagnetic below 715°K. In this case the magnetic moment of the octahedral Fe^{3+} dominates the antiparallel-oriented moment of the iron on tetrahedral sites, resulting in overall ferrimagetism.

It is better for us to first consider the factors that influence the cation distribution in spinels. Simply speaking, the cation distribution in spinel structures are related to some of

parameters, such as the interstices size, ions atomic radii, orbital preference for certain coordination and temperature [2]. The relative size of ions in comparison with the lattice size is the most effective factor. Trivalent ions are normally smaller than the divalent due to the formation of greater electrostatic attraction in the larger charge and results in the outer orbits to pull inward. With these considerations, however, it was not always able to obtain a consistent picture of the cation distribution as found experimentally. For instance, it is known that Zn^{2+} and Co^{2+} have equal ionic radii, but they own different structure. $CoFe_2O_4$ is an inverse spinel while $ZnFe_2O_4$ is a normal spinel. This can be explained by an individual site preference of the various ions. Some ions may have a distinct preference for the octahedral site depending on the d-electron count. If the A^{2+} ions have a strong preference for the octahedral site, they will displace some of the B^{3+} ions from the octahedral sites to tetrahedral sites. Similarly, if the B^{3+} ions have a low octahedral site stabilization energy, they will occupy tetrahedral sites, leaving octahedral sites for the A^{2+} ions.

There is interaction between A and B sites in spinel ferrites, which to a huge extent influences their properties. The strength of interaction between the moments of different metal ions on the sites of A and B is determined by the distance between the oxygen ions and metal ions and the angle between them. The A-B configurations are the most ideal combination due to the shortest distance between the related ions and generation of 180 degree angle. When it comes to the A-A and B-B interactions, they are often viewed as the most unfavorable and weakest states, respectively [3]. Neel[4] described the ferromagnetism behavior of ferrites by consideration of A-B configurations. The net A and B magnetic moments are normally aligned in ferrites. Therefore, the discrepancy in the moments in the A and B sites result in partial

counteraction of the B sites moments by the A sites moments. The ferrimagnetism of Fe_3O_4 mentioned above is such an example.

We have already seen how intrinsic interaction and configurations affect properties of spinel ferrites. Besides, some morphological properties, such as porosity and density, grain size, and lattice constant, can also make a huge contribution.

Density and porosity play a key role in controlling the properties of polycrystalline ferrites. These two parameters are inversely proportional to one another and are functions of theoretical density of the material. According to Kim et al. [5], calcination temperatures can significantly influenced the final microstructure, especially density, thus varying the magnetic properties of the sintered ferrite. Any changes in ferrite's microstructure features would cause variation in the materials properties, which are commonly revealed by B–H or M–H curves. Porosity is an important microstructure feature limiting the movement of domain walls. Pores would appear to fix domain wall and restrict their movement [6]. A problem encountered in growing large grains in ferrite is that many pores will be crushed by the grain boundary and remain inside the larger grains during the process of growing large grains [7]. The intragranular porosity is more troublesome than the intergranular porosity. Guillaud [8] revealed that the permeability of Ni–Zn ferrite decreased with grain size exceeding 15 μm. It was concluded that this decrease was probably due to the induced porosity within the large grain. The presence of porosity within the grains results in the hindrance of the domain wall motion and is harmful to the initial permeability [9].

The grain boundaries and grain size can also influence properties. The permeability in ferrites, particularly for smaller grain sizes can be viewed as an example. The monodomain state will be made where no magnetic domain walls when small grains are formed eventually, which

can exist inside single grains [10]. Under this circumstance, it is clear that the grain size dependent permeability cannot be explained by phenomena related to domain walls. An attempt to understand the decreasing in permeability to smaller grains sizes was presented by Johnson and Visser [11]. In their non-magnetic grain boundary model, they assumed that grain boundaries consist of regions with low permeability which causes internal demagnetization fields. Within that model, the relative importance of the grain boundaries increases for decreasing grain size. However, it was not totally agreed by some other researchers.

The high resistivity of sintered ferrite could be dominated by the relatively high resistance of grain boundaries [12]. The conductivity and therefore the eddy current losses occurring at the high frequencies, for example, Mn–Zn ferrites in telecommunication application, depend strongly on the resistivity [13]. The eddy current loss can be reduced by increasing the resistivity of the material. The resistivity of the polycrystalline ferrite can be increased by increasing grain boundary resistivity and reducing grain size. For example, the presence of defects and the segregation of impurities to the grain interface can greatly increase the resistivity of the grain boundary [13]. The engineering of grain size and grain boundary tends to give different characteristics on the magnetic properties, which is an advantage to the researchers as this effect could be used to achieve the magnetic properties of desired materials.

Grain size, grain boundaries and porosity also affected the value of saturation induction and coercivity. The increased number of domains and easier movement of domain walls in larger grain with diminished grain boundaries result in high magnetization value. On the other hand, the presence of pores would hinder the movement of the domain walls, as mentioned before, thus reducing the magnetization. The coercivity value is very sensitive to porosity and grain size. It

8

was found to increase in single-domain grains until it reaches a maximum value and inversely proportional to the grain size for multidomain grains, as revealed in **Figure 2**.
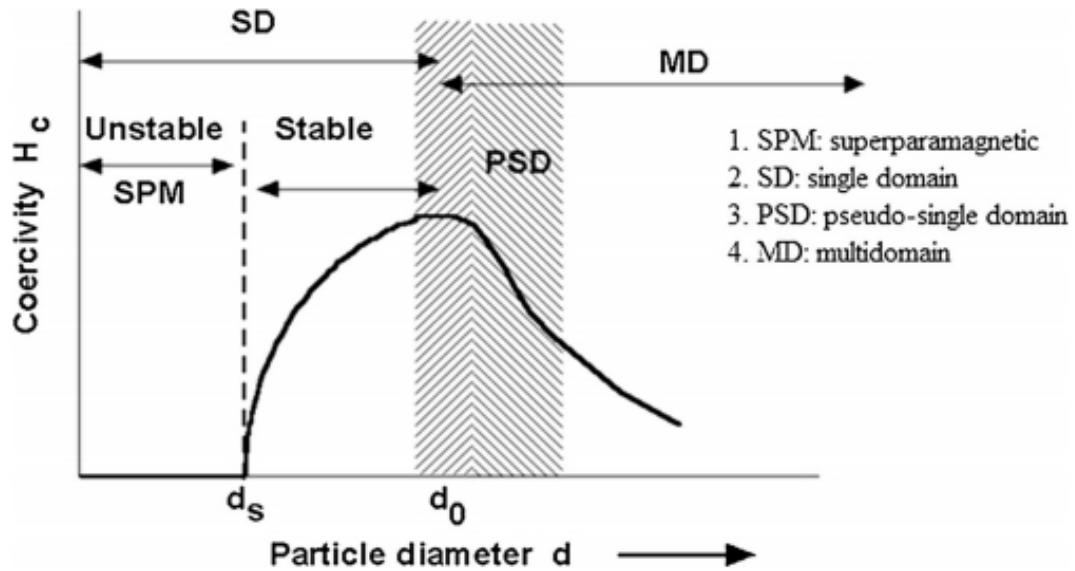
Fig. 2 Coercivity as a function of particle size [14]

Spinel ferrites are now widely used at present. One important reason is that ferrites are commonly cheaper than other materials, especially metal materials. When it comes to large-scale manufacture, choosing ferrites can greatly reduce production cost. In addition, ferrites well meets the demand for high-frequency stability, particularly in electric circuity. Core power loss of inductor components is often the limiting factor, so minimization of the core power loss has been of significant importance and a major pursuit of industry and academia in order to address the concerns associated with deployment of high efficiency and high power density equipment. When the conductor moves in a non-uniform magnetic field or is in a magnetic field that changes with time, the current generated inside the conductor causes the conductor to heat and produce

9

energy loss, which is called eddy current loss. Eddy current loss, which dominates at high frequency, can highly restrict performance of metals. As mentioned above, different from metals, ferrites own high resistance, greatly reduce the effect of eddy current.

There are many kinds of spinel ferrites applied in different fields. In this study, cobalt ferrites are our focus. Cobalt ferrites own unique physical, chemical, catalytic and magnetic properties. These ferrites show stable chemical performance, corrosion resistance and wear resistance, and is widely used in magnetic recording media, pigments, aerospace, magnetic sensors and so on. In addition, cobalt ferrites own high coercivity and resistivity, and also exhibit great permeability at high frequencies, so they are also commonly applied in the high frequency area. Besides, cobalt ferrite is a typical spinel ferrite which can show spinodal decomposition under specific conditions. This will be discussed later.

1.2 Synthesis

Synthesis route can significantly influence the microstructure and parameters of products, in our case, spinel ferrites, and this issue also involves the consumption of resources and energy. Therefore, choosing proper methods, improving and innovating techniques and procedure is of vital importance from aspects of demands, environment and economy. In this section, several methods will be introduced, and ball mill, which was used in our work, will be emphasized. Some information from our review article will also be involved [34].

1.2.1 Solid State Reaction

The term solid-state reaction route is commonly used to explain interactions where neither controlled vapor-phase interactions nor a solvent medium is carried out. The solid-state route is often employed where other methods are not sufficed, like the fabrication of refractory ceramics, glasses and bulk crystals. Moreover, this route is also applied to produce advanced materials with unique compositions. The solid-state method is known as the simplest way to form various materials. Applying this technique enables one to produce desired products by mixing high-purity oxide materials with certain proportion. However, some obvious disadvantages of the method may also be shown such as sintering at higher temperatures for long times (huge cost) and long milling time, and sometimes, it is difficult to control the process due to the formation of unwanted phases especially when producing metal-oxide composites.

A number of studies on solid-state synthesis of ferrites have been reported, among them doping is one of the most popular topic. Tokatlidis et al. [15] produced MnZn ferrite with Co^{2+} and Mg^{2+} as additives. Co^{2+} resulted in the reduction of power loss, although at the expense of lowering the initial permeability. The addition of Co broadens the B-B distances and impedes the conductivity between Fe^{2+} and Fe^{3+}. Additionally, the presence of Co^{2+} can stabilizes the Fe^{3+}, in that third ionization energy of Co^{2+} is higher than that of Fe^{2+}. Mg^{2+} stabilizes the resistivity in the high frequency region, and the conductivity of the ferrite is further hindered by the introduction of Mg^{2+}. The addition of Mg with a remarkably low melting point (650°C) is believed to promote the densification mechanisms, thus reducing energy barriers, such as pores or secondary phases, which are harmful to permeability.

Kalarus et al. [16] reported on solid-state reaction of Fe_2O_3, Mn_3O_4 and ZnO to produce high permeability MnZn ferrites. The authors carried a systematic study to optimize the processing conditions to enable (1) large grains necessary for high initial permeability, and (2) high grain boundary resistivity for exceptional frequency stability. The optimization is based on the homogeneous dissolution of dopants under oxidative conditions and their subsequent precipitation along grain boundaries. This was accomplished by integrating isothermal plateaus at the first part of the cooling stage of the final firing process.

Ni-Zn ferrite ($Ni_{0.64}Zn_{0.36}Fe_2O_4$) powder was synthesized from Fe_2O_3, ZnO and NiO via the conventional ceramic method by heating the stoichiometric amount of Fe_2O_3, ZnO and NiO at 1100°C for 2 h [17]. The average size of the Ni-Zn ferrite particle was is smaller than 5 μm. As shown in **Figure 3**, the magnetic loss in the Ni-Zn ferrite composite samples decreases as a result of increasing Ni-Zn ferrite amount, which proves that the contribution of the surrounding ferrite shell to reduce eddy current effects is effective. High-resistivity ferrite insulation coating of every iron particle with a high-resistivity ferrite produces tiny eddy current paths inside the particles and develops relatively high resistivity in the bulk material. In addition, the magnetic properties of high-resistivity Ni-Zn ferrite is also responsible for the low loss in the composites with high ferrite component, for instance, their permeability remains stable instead of dramatically dropping at high frequency.
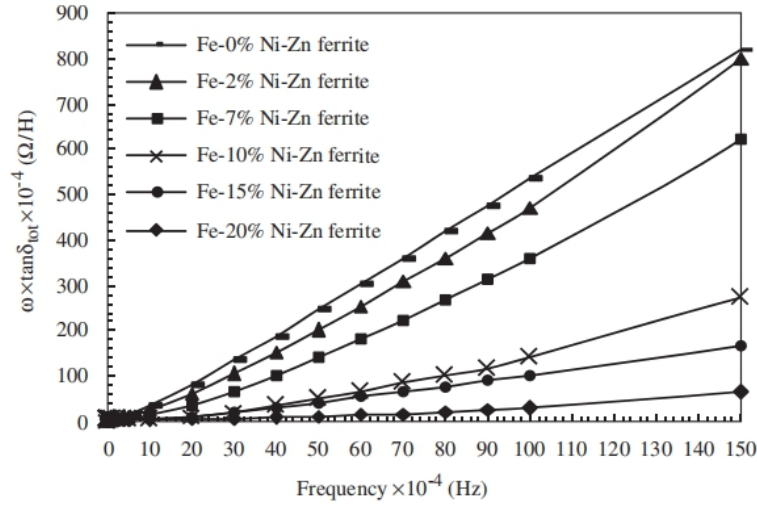
Fig. 3 Magnetic loss of Fe and Fe-Ni-Zn ferrite composite samples as a function of frequency [17]

Mechanical alloying method like ball mill is a good replacement for the solid state method with greater advantage of shortening the milling time. In this method apart from practicality, speeding up of material preparation of nanocomposites, advanced ceramics, amorphous alloys, metastables and other important powders in large tonnages are also achieved. The technique itself is easy and fast to get a desired product relatively in short time of milling. Therefore, it can save time and energy. These benefits made it a choice to prepare spinel ferrites, which will be discussed in detail in next section.

1.2.2 Ball Mill

Ball mill is a powder processing technique that allows production of homogeneous materials starting from blended elemental powder mixtures. The technique has been used to produce a variety of soft magnetic composites. Essentially two processing routes are carried out: the first involves reactive milling of precursor oxide mixtures, and the second applies traditional powder techniques either wet or dry milling to form nanostructured materials.

Rashidi et al. [18] synthesized polyvinyl alcohol/cobalt ferrite nanocomposites upon employing a two-step procedure: the spherical single-phase cobalt ferrite of 20-4 nm mean particle size was synthesized via mechanical alloying method and then embedded into polymer matrix by intensive milling. Magnetization and coercivity of produced samples have been decreased in comparison to pure cobalt ferrite as a result of the presence of non-magnetic polymer layer.

Moustafa et al. [19] reported on preparation of Mg ferrite by either mechanical milling only, or mechanical milling followed by sintering. In the latter case, Mg-ferrite has been produced at relatively low temperature or with short heating times.

$CoFe_{1.95}Ho_{0.05}O_4$ spinel ferrite was produced by mechanical alloying from Fe_2O_3, CoO and Ho_2O_3 followed by annealing [20]. The magnetic grains showed single domain or pseudo-single domain behavior below the critical annealing temperature 1050°C above which grains became multi-domains. Consequently, a significant transformation in the magnetic behavior of the material was noted around 1050°C, with changes in magnetic parameters as a result of increasing the grain size. The added Ho^{3+} occupies B site, which means there is a replacement of antiferromagnetic $Fe^{3+}(B)$-O-$Co^{2+}(B)$ interactions by the equivalent amount of ferromagnetic Fe^3

14

$^+$(B)-O-Ho^{3+}(B) interactions. The substantial enhancement of T$_C$ in CoFe$_{1.95}$Ho$_{0.05}$O$_4$ spinel ferrite, in spite of expected weaker exchange interaction between Fe^{3+} (3d) and Ho^{3+} (4f) ions, suggest that a strong superexchange (A-O-B) interaction appears between A site (Fe^{3+}) and B site (Fe^{3+}/Co^{2+}) moments in the presence of Ho^{3+} ions, which enhanced the magnetic property.

Milling atmosphere is another critical factor affecting the resultant composites. Due to the interaction between the grinding balls and powder, the mechanical energy is converted into heat so that temperatures inside the ball mill pot rise substantially which means it is much easier to react with oxygen. Therefore, mechanical alloying of soft magnetic composites is typically processed under inert gases such as argon. Ding et al. [21] operated ball milling to form Mn ferrite in air and under Ar separately. The product milled in air contained plenty of oxide impurity, while the sample milled under Ar reached single phase. Equally important is the milling media and powder agglomeration where stearic acid, solid paraffin, liquid alcohol and carbon tetrachloride, are often used as a milling media in order to reduce the agglomeration of powder.

Fe-Ni nanocrystallite powders display particularly interesting soft magnetic properties such as low coercivity and high saturation magnetization. Koohkan et al. [22] studied the milling time effect on magnetic properties of Fe-Ni nanocrystallite powders. Increasing the milling time (up to 100 h) has resulted in decreasing the crystallite size, whereas microstrain and lattice parameters have increased. A trend in the coercivity increase with milling time (up to 100 h) as well as the intrinsic flux density increases has been observed.

As technology is developing, some ball milling machines with higher efficiency has been used more frequently, which is known as high energy ball milling. Difference between high-energy ball milling and traditional low energy ball milling is that the speed of the balls of high-

energy ball milling is higher, promoting plastic deformation and phase transformation, otherwise the traditional ball milling process can only have crush and mix. High-energy ball milling's energy utilization rate is greatly increased, so as to improve the performance of the material, is a kind of energy-saving and efficient material preparation technology, and has become one of the important methods for the preparation of nanometer materials. **Figure 4** shows the planetary ball milling machine which is used in this work. Planetary ball mills are usually smaller than common ball mills and mainly used in laboratories for grinding sample material down to very small sizes. A planetary ball mill consists of at least one grinding jar which is arranged eccentrically on a so-called sun wheel. The direction of movement of the sun wheel is opposite to that of the grinding jars (ratio: 1:−2 or 1:−1). The grinding balls in the grinding jars are subjected to superimposed rotational movements, the so-called Coriolis forces. The difference in speeds between the balls and grinding jars produces an interaction between frictional and impact forces, which releases high dynamic energies. The interplay between these forces produces the high and very effective degree of size reduction of the planetary ball mill.

Fig. 4 Retsch Planetary Ball Mill PM 100

Ball mill is a simple synthesis method to form spinel ferrites. In addition, defects are easily induced during ball mill, resulting in higher diffusion rate, which may promote spinodal decomposition.

1.2.3 Other Methods

Sol–gel method is one of the commoly used wet chemical methods to produce magnetic ferrites. In this chemical procedure, a "sol" (a colloidal solution) is formed that then gradually evolves towards the formation of a gel-like diphasic system containing both a liquid phase and solid phase whose morphologies range from discrete particles to continuous polymer networks.

The reaction initiates from a chemical solution which owns characters as the precursor for gel of either network polymers or discrete particles. Normally, metal chlorides and metal alkoxides in different forms of polycondensation and hydrolysis are being used as a precursor. During the process, metal oxides are formed by joining the metal centers with hydroxo (M–OH–M) or oxo (M–O–M) bridges, thereby producing metal-hydroxo or metal-oxo polymers in solution.

Zahi et al. [23] used a sol–gel method to synthesize a NiZn ferrite nanocrystalline by dissolving the metal acetates in acetic acid. Their results showed that a desired ferrite was formed after heating at 600 ℃ for 4 h. Their findings revealed that by performing this technique, it can reduce a synthesis temperature, minimize the zinc evaporation and achieve high purity of final products. Atif et al. [24] also performed the sol–gel technique to produce NiZn ferrite nanoparticles. The gel was prepared from the chemical reagents of metal nitrates and citric acid. The gel attained was fired at 200 ℃ followed by sintering the loose powders at 500 ℃ for 3 h. The nanosized particles of $NiFe_2O_4$ synthesized by the sol–gel method could be sintered at a lower temperature as compared to its solid-state counterpart. The sintering behavior of $NiFe_2O_4$ nanoparticles is much superior compared to coarse-grained powder obtained through the solid state reaction process [25]. The major advantages of sol-gel method are a low synthesis temperature, energy saving, high purity, small and uniformed particle sizes as well as homogeneous distribution. However, this technique is being relatively new and it owns some drawbacks. For instance, this method is environmentally unfriendly because of the toxicity of some of the alcohols utilization. Another drawback of this method is the high cost of raw chemical materials, and sometimes, the segregation may occur during gel formation in the used dopants. Moreover, high temperature is needed to eliminate the residual hydroxides from the products.

Another method, the precipitation, is the settling down by a precipitate of substances normally soluble under the conditions employed. It includes the simultaneous precipitation of required hydroxides from a solution so that the precipitate contains the required metals in the desired proportion. The prepared solution is the mixture of dissolved precipitation agent like ammonium hydroxide or ammonium oxalic and oxalic acid to precipitate the blended hydroxide or oxalate as well as the combined hydroxide or oxalate out of solution. By heating the precipitates at higher temperatures, the final crystalline oxide is attained. Many researchers have carried out the precipitation method to produce spinel ferrites nanoparticles. Sharifi et al. [26] prepared CoZn ferrite using co-precipitation technique and sintering at 1000 °C. The ferrite crystallite size was in the range of 6-10 nm. In another study, Jahanbin et al. [27] prepared a high-purity NiZn ferrite by precipitation. They showed that by performing this method, it is possible to form a spinel ferrite at shorter duration than that required in the conventional method.

Generally speaking, synthesis methods of spinel ferrites can be divided into two main groups, which are non-conventional and conventional methods. The non-conventional powder processing in a liquid/solid medium, such as sol-gel, may produce intermediate, finely divided mixed hydroxides or mixed organic salts to assist in the subsequent diffusion process. When it comes to conventional methods, the starting materials are conventionally oxides or precursor of oxides of the cations. This process involves the interdiffusion of the various metal ions of preselected compositions to form a mixed crystal. In other words, the techniques of preparing nanocrystalline spinel ferrites are categorized into two: chemical and conventional solid-state routes. Each of them has its own benefits and drawbacks. For example, by applying the chemical

methods, it is possible to produce a finer crystallite size as well as synthesize at lower temperatures as compared to the conventional solid-state routes. However, it is believed that the chemical homogeneity of the gel is often disturbed by the differences in the chemistries of the cations. On the other hand, the conventional solid-state routes are relatively simple techniques, but the control of particle size and powder quality during the process sometimes is difficult. Furthermore, the synthesis of them sometimes needs higher temperature, and as a result, an expensive furnace is required. Furthermore, the non-conventional techniques may have environmental drawbacks, but the high temperatures required in conventional sintering also carried a significant carbon footprint.

1.3 Phase Decomposition

Binodal decomposition is a kind of phase decomposition based on nucleation and growth mechanism, and it is known to occur in between spinodal and binodal curve (i.e. miscibility gap), which is shown in **Figure 5(a)** [28]. Nucleation is the first step in the formation of a new thermodynamic phase, then followed by growth. Generally, when the second derivative of the free energy with respect to the components is greater than 0, there is a certain barrier need to be overcome in order to form a stable nucleus, at this point phase decomposition obey nucleation-growth mechanism, and binodal decomposition occurs. This mechanism is characterized by a large degree of initial concentration variation and a small spatial range involved.

The nucleation-growth model works for the description of phase formation starting from metastable initial states, while thermodynamically unstable states are believed to decay via

spinodal decomposition. Spinodal decomposition is a process by which a homogeneous solution inside a miscibility gap spontaneously decomposes into a mixture of two phases. This process is fundamentally different from nucleation and growth. When there is a nucleation barrier to the formation of a second phase, the system takes time to overcome that barrier. As there is no barrier to spinodal decomposition, some fluctuations start growing instantly. Infinitesimal compositional fluctuations in the unstable homogenous solution lower Gibbs free energy and proceed until resultant phases are in an equilibrium state. Moreover, in spinodal decomposition fluctuations start growing everywhere, uniformly throughout the volume, whereas a nucleated phase form at a discrete number of points. Different co-existence behaviour of spinodal decomposition and binodal decomposition(nucleation) is shown in **Fig. 5(b) and 5(c)**, and T-c phase diagram is shown schematically in **Fig. 5(a)** [28]. The miscibility gap, which refers to the curve outside nucleation area, and the spinodal curve, which is the curve separating spinodal decomposition area and nucleation area, are found by equating the first and second derivatives of the ΔG_{mix} respectively to zero.
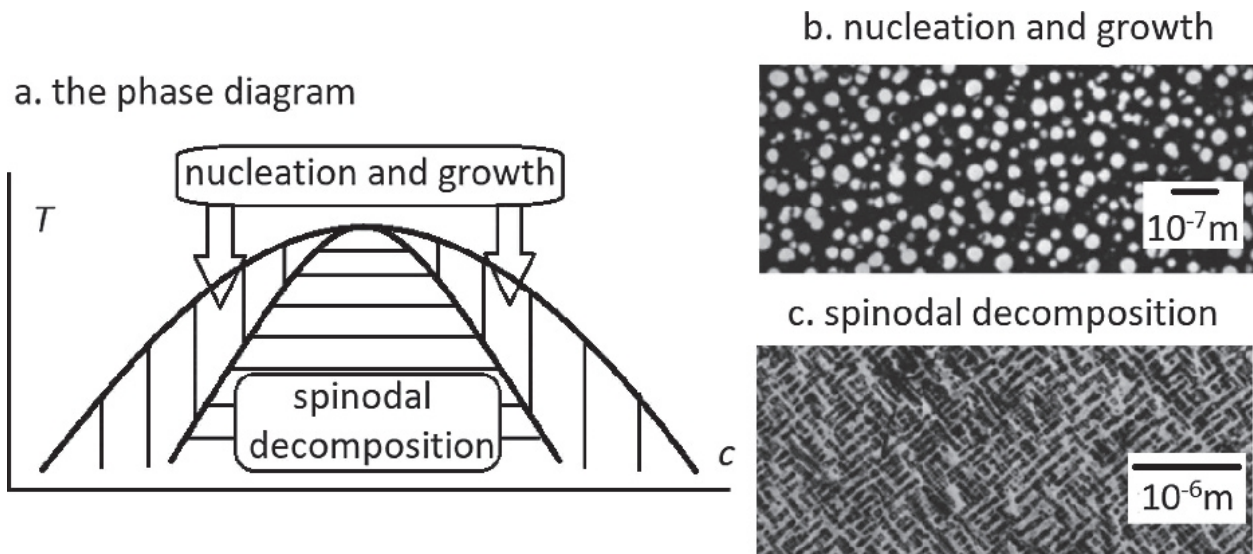
Fig. 5 (a) Schematic phase diagram of a binary alloy displaying a miscibility gap; (b) TEM dark field image of precipitates in Ni－37at.%Cu－8at.%Al aged for 167 h at T = 580 ◦C; (c) TEM bright field image of Cu－36at.%Ni4at.%Cr aged for 240 h at T = 650 ◦ C displaying particle alignment along the <100> matrix directions [28].

The mechanism type can affect shape, size and relative position of the second phase precipitates at the final stage of the decomposing process. An example of typical precipitates formed by the nucleation and growth mechanism illustrated in **Figure 5(b)**, showed discrete structures. In contrast, the typical precipitates formed by the spinodal mechanism, illustrated in **Figure 5(c)**, represent periodic modulated structures.

Spinodal decomposition was first studied in alloy, and then researches on ceramics emerged. Spinodal decomposition in cobalt ferrites has been reported upon several synthesis routes, like sol-gel, solid-state routes and precipitation, and many characterization techniques have been used to prove the presence of spinodal decomposition. Takahashi et al. [29] studied microstructural

changes using XRD and TEM. Occurrence of the phenomenon upon aging was characterized by the appearance of side bands in XRD pattern, implying a modulated structure. After further aging, separation between side bands decreased and finally disappeared and two discrete bands were observed, implying loss of coherency. TEM analysis revealed the presence of period microstructures with confirmed spinodal decomposition.

Many researched were performed to find evidence of spinodal decomposition. Le Trong et al. [30] studied the phase decomposition process in the cobalt ferrites. The precipitates were subjected to two kinds of heat treatments. One is calcinated at 900 °C in single phase field followed by air quench and subsequent firing at 700 °C inside the miscibility gap, and the other is direct calcinated at 700 °C inside the miscibility gap. Early stages of decomposition during former route proceeded via spinodal decomposition as revealed by the presence of Moire fringes in TEM pattern amd modulated structures in HRTEM investigations. **Figure 6** shows TEM micrograph of sample annealed at 700 °C for 36h. Moire fringes appeared, which indicates overlap of different phases.
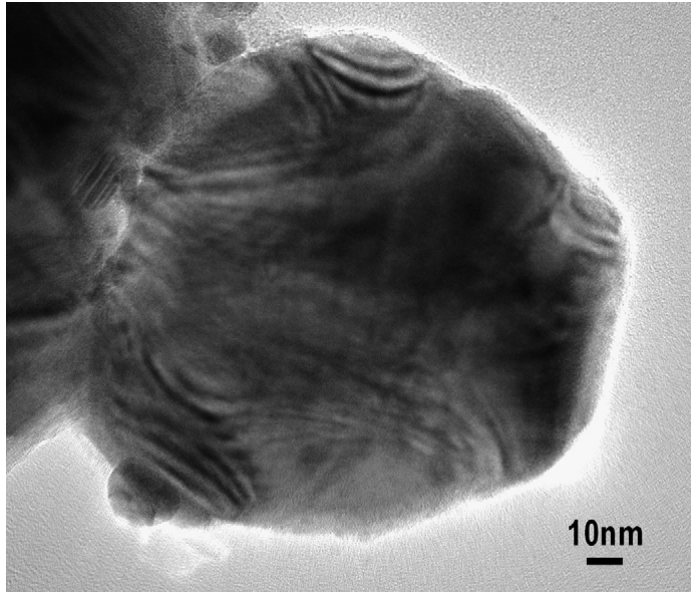
Fig. 6 TEM micrographs of samples prepared at 900 °C and annealed 36 h at 700 °C showing Moiré fringes in different places within the crystal [30].

In addition, side bands in XRD patterns also showed up. These modulated structures disappeared with annealing time increasing and two distinct incoherent Co-rich and Fe-rich phases appeared instead. However, in latter route, no spinodal decomposition was observed. Calcinated at 900 °C resulted in the formation of a single phase which was unstable during firing at 700 °C. However, when directly calcinated at 700 °C, no such phase was present and hence nucleation and growth took the lead instead of spinodal decomposition.

1.4 Analysis Tools

In this section, some characterization techniques commonly used in research on spinel ferrites will be simply introduced.

1.4.1 XRD

XRD is the abbreviation for X-ray diffraction. It is known that crystals are regular arrays of atoms, and X-rays can be considered waves of electromagnetic radiation. Atoms scatter X-ray waves, primarily through the atoms' electrons. Just as an ocean wave striking a lighthouse produces secondary circular waves emanating from the lighthouse, so an X-ray striking an electron produces secondary spherical waves emanating from the electron. This phenomenon is known as elastic scattering, and the electron (or lighthouse) is known as the scatterer. A regular array of scatterers produces a regular array of spherical waves. Although these waves cancel one another out in most directions through destructive interference, they add constructively in a few specific directions, determined by Bragg's law. These specific directions appear as spots on the diffraction pattern called reflections. Thus, X-ray diffraction results from an electromagnetic wave (the X-ray) impinging on a regular array of scatterers (the repeating arrangement of atoms within the crystal). If structure of crystals is known, the wavelength of the X-ray can be calculated after the direction θ of the diffraction line is determined, thus determining the element that produces the characteristic X-ray. This is called X-ray spectroscopy, and can be used to analyze the composition of materials.

XRD is a fundamental analysis method in research on spinel ferrites. Composition, lattice parameter, and crystallographic structure of spinel ferrites can be determined via XRD technique.

In addition, it is also a useful method to prove spinodal decomposition. Side band in X-Ray Diffraction (XRD) patterns is viewed as evidence of spinodal decomposition, as shown in **Figure 7**.
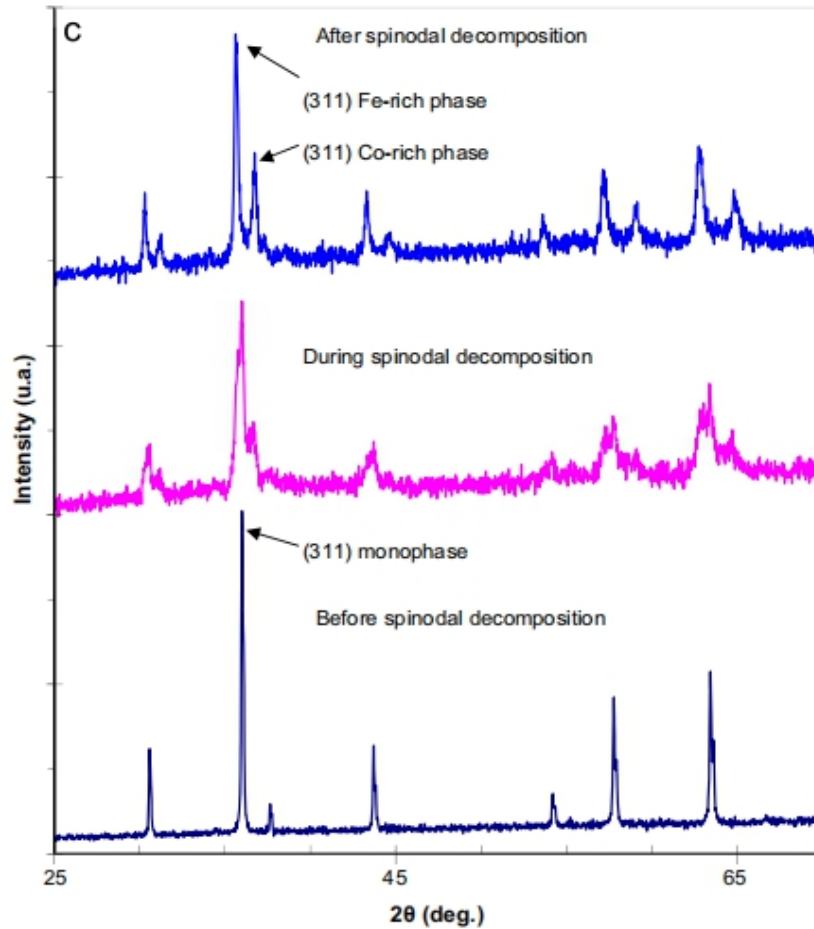
Fig. 7 XRD pattern of Co$_{1.73}$Fe$_{1.27}$O$_4$ powder quenched at 900 °C and annealed at 700 °C 36 h and 120 h [31]

1.4.2 SEM

A scanning electron microscope (SEM) is a type of electron microscope that produces images of a sample by scanning the surface with a focused beam of electrons. The electrons interact with atoms in the sample, producing various signals that contain information about the

26

surface topography and composition of the sample. The electron beam is scanned in a raster scan pattern, and the position of the beam is combined with the intensity of the detected signal to produce an image. In the most common SEM mode, secondary electrons emitted by atoms excited by the electron beam are detected using a secondary electron detector, which is called Everhart-Thornley detector. The number of secondary electrons that can be detected, and thus the signal intensity depends on specimen topography. Some SEMs can achieve resolutions better than 1 nanometer.

We can obtain a general understand of morphology of microstructure. The arrangement of particles, the shape and size are clearly shown in SEM images. For instance, as shown in **Figure 8**, the microstructural comparison presented the homogeneity and high purity in the sol-gel samples and the smaller grains confirmed the finer particles [32].
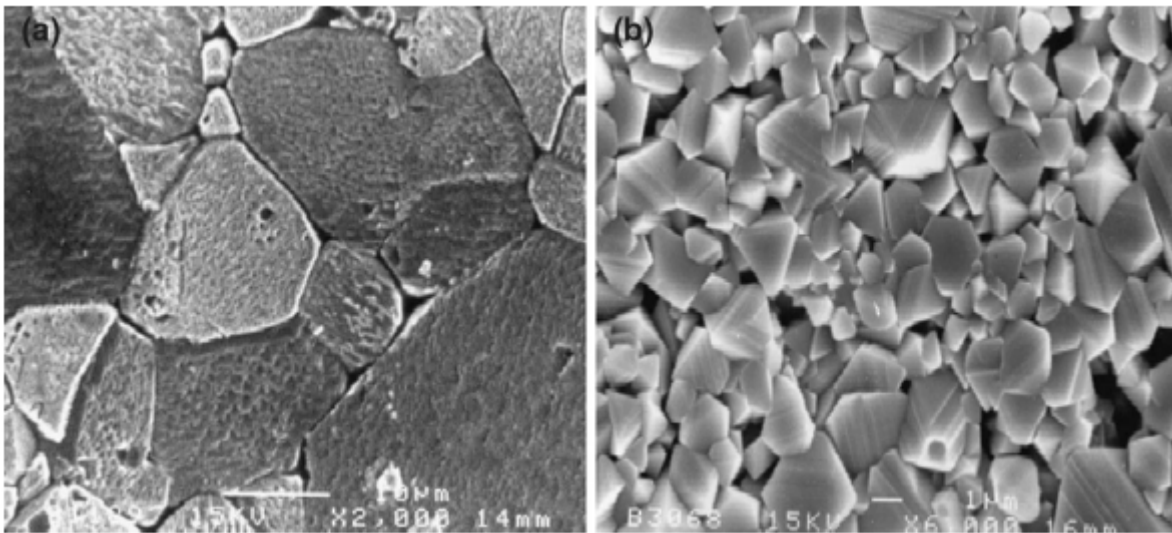

Fig. 8 Microstructure of Ni–Zn ferrite samples prepared by a solid-state reaction, b sol–gel route [32]

1.4.3 VSM

The vibrating sample magnetometer (VSM) is one of the most successful implementations of a magnetometer. In comparison with alternating gradient magnetometer, the VSM is indifferent to mass and size of sample up to a considerable range. In this scheme the sample is introduced in a constant uniform external magnetic field which induces a magnetisation in the sample. As the magnetized sample is then vibrated, it introduces perturbations in the external magnetic field. A set of coils or some magnetic field sensors can be arranged around the sample to measure these perturbations. For example in the case of coils, magnetic flux piercing the coils will change resulting in generation of an emf (electro motive force) in coils. For a particular coil geometry, the emf generated in coils will depend on (a) the amplitude and frequency of vibration, (b) external magnetic field and (c) the magnetization of sample. With proper manipulation, we can deduce the value for magnetisation from emf. A schematic for VSM is shown in **Figure 9** [33].

When we study spinel ferrites, we need VSM to obtain magnetic parameters, such as coercivity, hysteresis and magnetic saturation, which is important for understanding the magnetic properties of spinel ferrites.
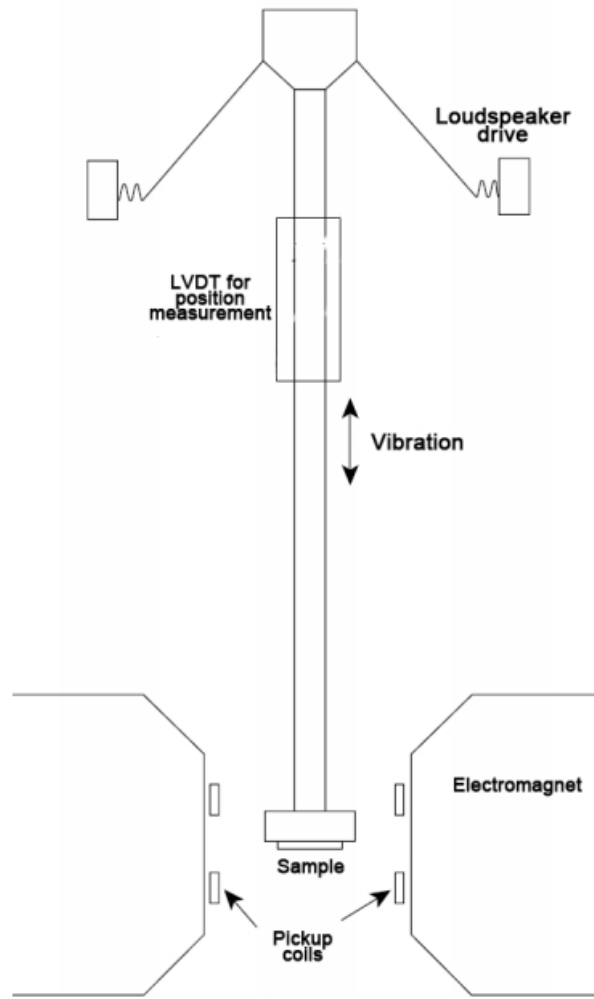
Fig. 9 VSM [33]

2.0 Research Description

2.1 Hypothesis

Spinel ferrites can undergo phase decomposition inside miscibility gap and form different new phases, which are ferromagnetic phase and nonmagnetic phase. These mixed new phases will greatly impact the magnetic property of spinel ferrittes, and the decomposition behavior will be significantly influenced by composition and processing.

2.2 Objectives

To find out how composition and processing such as annealing influence the phase decomposition, we synthesized different samples under various conditions. We took advantages of several analytic instruments to characterize these samples in order to learn how magnetic properties changed during decomposition and the influences of different process conditions and composition.

2.3 Tasks

In this research, magnetic parameters such as coercivity and saturation magnetization should be compared. In addition, parameters related to structure and composition like particle size, phase peak and lattice constant are also important to learn the influences.

There are some key points during the research that we need to notice. The first is that we should carefully synthesize various samples to achieve high-quality spinel ferrites products, especially when perform ball milling. Ball milling, as a simple mechanical alloying method, may result in inhomogeneous mixing of powder, and aggregation as well. High-quality products will make our result more credible.

3.0 Experiment Procedure and Details

In order to study influences of different conditions on phase decomposition behaviour and magnetic property, we made several groups of samples with different milling time, calcination temperature, annealing time and Co-Fe ratio. All samples and detailed conditions are showed in **Table 1**. It is important to note that compositions outside the brackets were based on weight of raw materials, and compositions inside the brackets took iron added during ball mill into consideration, which are closer to real compositions.

Table 1 Samples made under different conditions

Sample No.	Composition	Milling time	Calcination temperature($^\circ$C)	Annealing Time
01	$Co_{1.7}Fe_{1.3}O_4$	6h	0	0
02	$(Co_{1.54}Fe_{1.46}O_4)$		700	0
03			900	0
04				36h
05		16h	0	0
06			900	0
07				36h
08				120h
09		30h	0	0

Table 1 (continued)

Sample No.	Composition	Milling time	Calcination temperature(℃)	Annealing Time
10	$Co_{1.7}Fe_{1.3}O_4$	30h	900	0
11	$(Co_{1.54}Fe_{1.46}O_4)$			36h
12	Co_2FeO_4	16h	0	0
13	$(Co_{1.8}Fe_{1.2}O_4)$		900	0
14				36h
15	$Co_{1.9}Fe_{1.1}O_4$	16h	0	0
16	$(Co_{1.75}Fe_{1.25}O_4)$		900	0
17				36h
18	$Co_{2.1}Fe_{0.1}O_4$		0	0
19	$(Co_{1.94}Fe_{1.06}O_4)$		900	0
20				36h
21	$Co_{2.5}Fe_{0.5}O_4$		0	0
22	$(Co_{2.32}Fe_{0.68}O_4)$		900	0
23				36h

3.1 Ball Milling

Solid solution Fe-Co-O system was first formed via planetary ball milling. The stoichiometric amount of high purity Fe_3O_4 and Co_3O_4 were mixed to obtain the composition $Co_xFe_{3-x}O_4$ shown in **Table 1**. The mixed powder and the steel balls (5 mm) were taken into the steel bowl (125 ml). The ball to material ratio was maintained at 8:1. The mixed powder was subjected to high-energy mechanical milling using Retsch planetary ball mill PM 100, and we chose ethanol (25 mL) as dispersant. The milling was continued at rotational speed 450 rpm, and we applied different milling time as **Table 1** reveals. After milling, we dried the products we got and performed grinding, then conserved these samples.

3.2 Calcination and Annealing

We performed calcination after ball milling via Lindberg Blue M tube furnace in air. Different calcination temperature were applied at 700 °C and 900 °C for 12 h. Afterwards, samples were annealed in tube furnace in air at 700 °C for different time as **Table 1** notes.

3.3 Characterization

Structural characterization of our powder was performed at room temperature using Bruker D8 XRD system. The copper Kα X-ray radiation ($K_{\alpha 1}$ = 0.15405 nm and $K_{\alpha 2}$ = 0.15443 nm) was used for the diffractometer.

Imaging and elemental analyses were performed using a Apreo scanning electron microscope (SEM) operating at 200 kV and equipped with an X-ray energy dispersive spectroscopy (X-EDS) system.

The magnetic properties were measured at room temperature using a 8600 series vibrating sample magnetometer (VSM) from Lake Shore Cryotronics. The maximal applied field for the measurements was 5 kOe. Particle size of our powder samples was measured using HORIBA LB-550 DLS.

4.0 Results and Discussion

Based on some calculation on phase decomposition behaviour, people have got specific phase diagram to describe decomposition in Fe-Co-O system. **Figure 10** is temperature vs. composition diagram. The dot line is spinodal curve, and the solid line under 900 °C is binodal curve, which is also called miscibility gap.
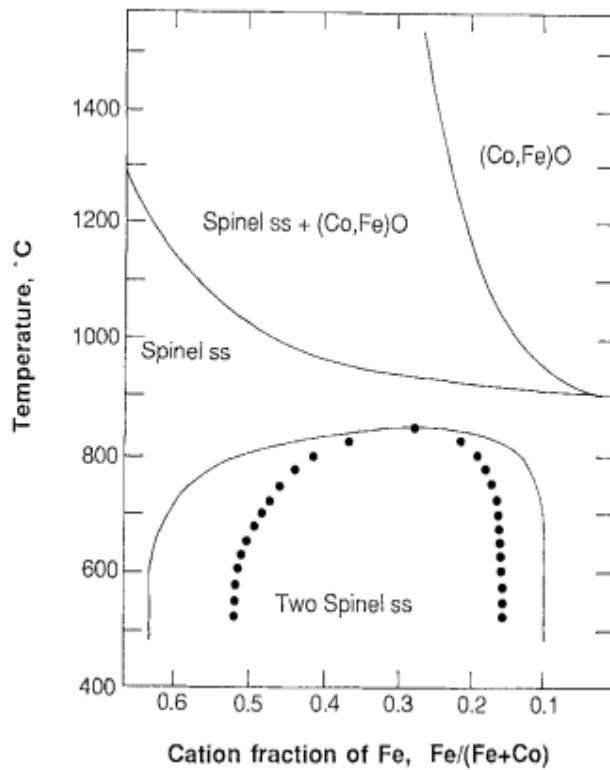
Fig. 10 phase diagram of Fe-Co-O system [29]

As mentioned in **chapter 1.3**, spinodal decomposition tends to dominate inside spinodal curve, and nucleation takes the lead in between spinodal curve and miscibility gap. In order to

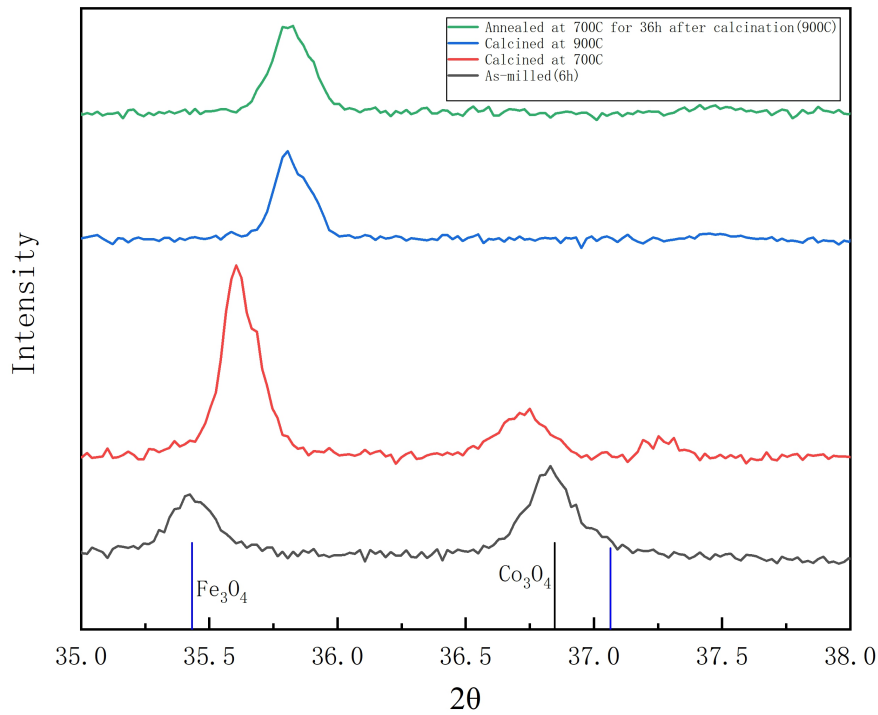get most clear result, we choose 700 °C as annealing temperature since it owns relatively broad space inside spinodal curve and high chemical energy which makes decomposition much easier. Also, we first formed $Co_{1.7}Fe_{1.3}O_4$ in that such Fe-Co ratio is near center of spinodal area, so that we can observe obvious decomposition behavior. However, when we perform ball milling, we need to take the weight loss of steel balls into consideration. During milling, Fe of balls dissolved into Fe-Co-O solution making Fe-Co ratio increased. Consequently, the overall composition shifted to spinodal curve boundary, making its decomposition behaviour different. Afterwards, we produced several samples with different Fe-Co ratio distributed in different areas inside spinodal curve to observe their behaviour. Accordingly, our discussion will be divided into two parts, based on composition near spinodal curve boundary and in center of spinodal area.

4.1 Composition Near Spinodal Curve Boundary

We added 5.763 g Co_3O_4 and 4.237 g Fe_3O_4 to form $Co_{1.7}Fe_{1.3}O_4$, and the real composition is expected to be around $Co_{1.54}Fe_{1.46}O_4$ when we take weight loss of steel balls during milling into consideration. 11 samples with such composition are made under different condition, which are marked from sample 01 to sample 11 shown in **Table 1**. We will discuss how these different conditions influence decomposition behaviour and property below.

4.1.1 Calcination Temperature

Sample 01, 02, 03, 04 which were all under 6 h ball milling, are used to figure out how calcination and distinct calcination temperature make a difference. It is clearly shown in **Table 1** that we calcined sample 02 at 700 ℃, and sample 03 and 04 at 900 ℃, then sample 04 experienced being annealed at 700 ℃ for 36 h after calcination.

Fig. 11 XRD result of Sample 01, 02, 03 and 04 (from bottom to top)

Figure 11 shows XRD result of these samples. It can be clearly seen that two components mixed together after 6h ball milling but there was no new phase formed. After calcination at 700 ℃, the two main peaks which represent Fe_3O_4 and Co_3O_4 got closer, and a new peak shows up around 37.3°. This new peak probably derived from Fe_3O_4 secondary peak

around 37.07°, which is marked by blue line in standard spectra on the bottom, since it shows similar shift behaviour to main peak of Fe_3O_4 around 35.7°. Obviously, the Fe-Co-O solid solution after calcination at 700 °C is a mixture of three phases--Fe_3O_4, Co_3O_4 and $Co_xFe_{3-x}O_4$. Differently, when calcination temperature increased to 900 °C, the Fe-Co-O solid solution shows single phase structure, which only contains $Co_xFe_{3-x}O_4$. These results are consistent with phase diagram shown in **Figure 10**. Sample 04 was annealed at 700 °C for 36 h after calcination at 900 °C. It is revealed that main peak got slight broader after anneal, but no other significant evidence for spinodal decomposition was found in XRD patterns.
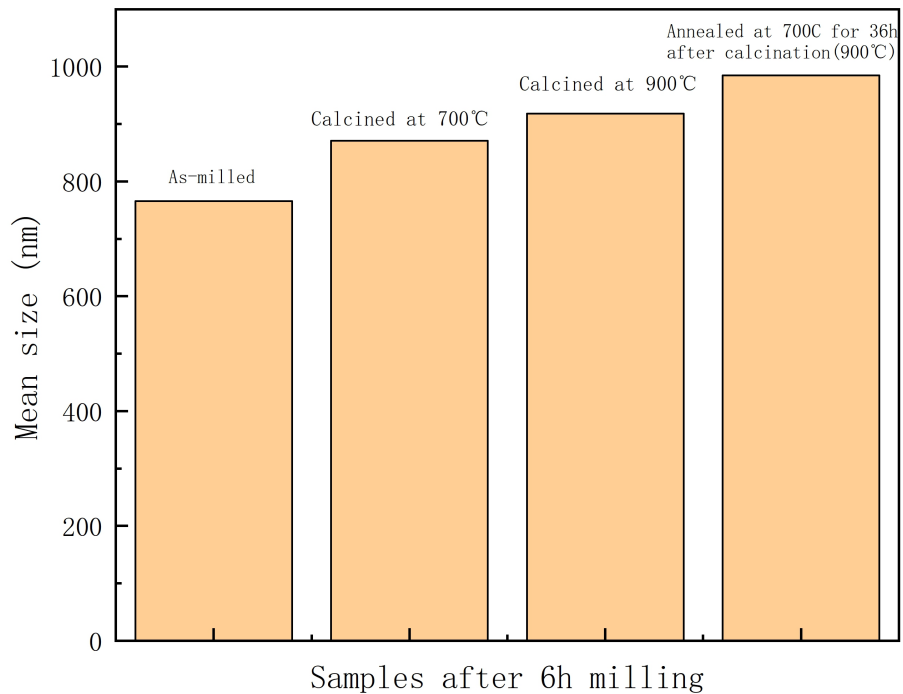
Fig. 12 Mean particle size of sample 01, 02, 03 and 04 (from left to right)

We performed DLS test on these four samples to obtain their particle size, and the result is revealed in **Figure 12**. After calcination, particle size slightly increased, and kept increasing with higher calcination temperature and longer treatment time. The increase of particle size mainly result from growth of particles during calcination and anneal, which is greatly influenced by thermal conditions.
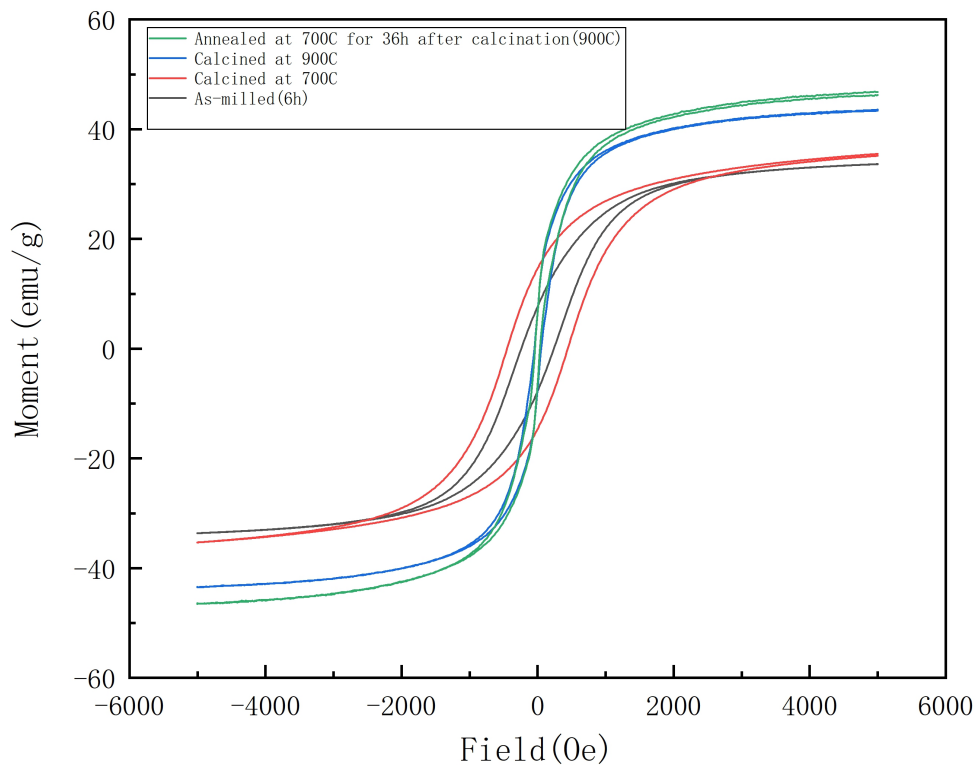
Fig. 13 Hysteresis loops of sample 01, 02, 03 and 04

**Table 2 Coercivity and Saturation Magnetization of Sample 01, 02, 03 and 04**

	Sample 01	Sample 02	Sample 03	Sample 04
Coercivity (Oe)	242.4	447.49	50.34	47.34
Saturation Magnetization(emu/g)	33.61	35.49	43.55	46.80

Result of VSM test is shown in **Figure 13**, and some detail parameters are revealed in **Table 2**. Intriguingly, different calcination temperature has huge influence on magnetic behavior and property. Besides, we made a simple calculation based on Bohr magneton and spinel structure to estimate contribution of Co_3O_4, Fe_3O_4 and $Co_xFe_{3-x}O_4$ on M_s value. Estimated M_s of pure Co_3O_4, Fe_3O_4 and $CoFe_2O_4$ is 0, 92 and 90 emu/g, separately. As-milled powder shows low saturation magnetization (M_s), since it contains nonmagnetic phase Co_3O_4. After calcination at 700 °C, saturation magnetization got a bit higher, in that a small quantity of $Co_xFe_{3-x}O_4$, which gave a positive value to M_s, was formed. Coercive field increased as well, probably result from growth of grains and mixture of three phases which increased magnet anisotropy. When calcination temperature increased to 900 °C, shape of hysteresis loop shows typical character of soft magnetic materials--it turns taller and thinner, which means the single phase ferrites got higher saturation magnetization and lower coercive field. Formation of single phase decreased magnet anisotropy, which mainly caused the sharp drop of coercivity, and based on our calculation, its M_s should be higher than mixture of Co_3O_4 and Fe_3O_4, which is consistent with our result. After being annealed at 700 °C, M_s increased slightly and coercive field almost kept the same value. Combined with the information we got from XRD analysis, phase separation

hardly took place in this case, and the higher saturation magnetization may credit to larger grain size formed during anneal, since domain wall motion got easier in larger grain size.

4.1.2 Annealing Time

Sample 05, 06, 07 and 08 were all milled at 450 rpm for 16h. It is clearly revealed in **Table 1** that sample 05 was simply milled; sample 06 was calcined under 900 ℃ for 12h after milling; sample 07 was annealed at 700 ℃ for 36h after calcination; and sample 08 was annealed at 700 ℃ for 120h. This group of samples was made to study how different annealing time influences cobalt ferrites.
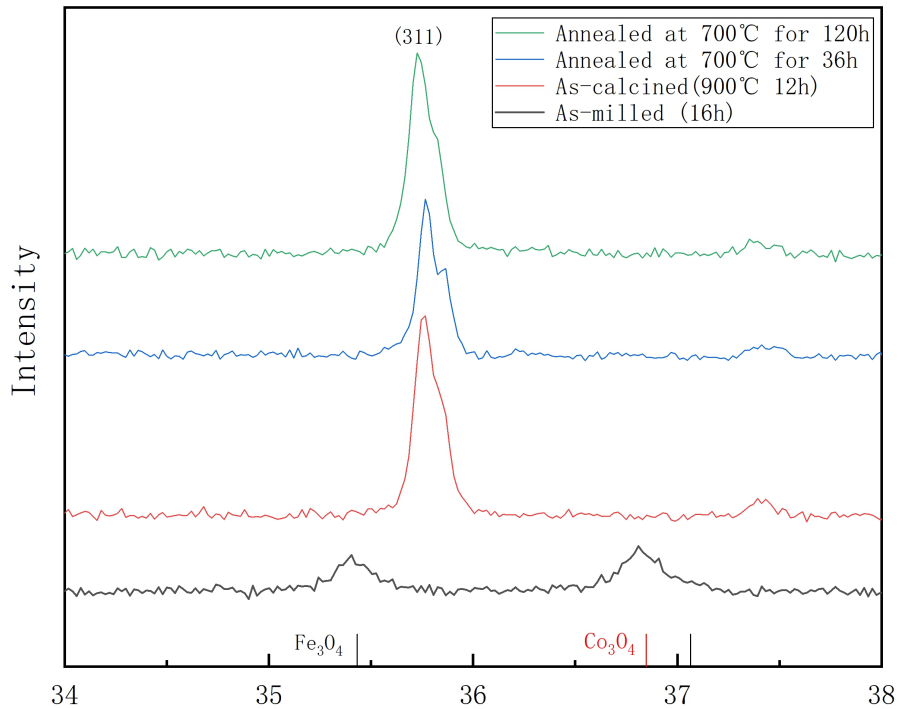
Fig. 14 XRD result of Sample 05, 06, 07 and 08 (from bottom to top)

Fig. 14 shows the result of XRD analysis of sample 05, 06, 07 and 08. After calcination at 900 ℃, single phase structure was formed, as discussed in last section. With annealing time increased, the main peak around 35.7° became slightly broader and a small left shift took place, but no obvious peak separation observed. In addition, when annealing time increased to 120h, a peak split can be observed at secndary peak around 37.5°. These information may tell that phase decomposition took place during long time annealing process, and the decomposition behaviour involves both spinodal decomposition and binodal decomposition.
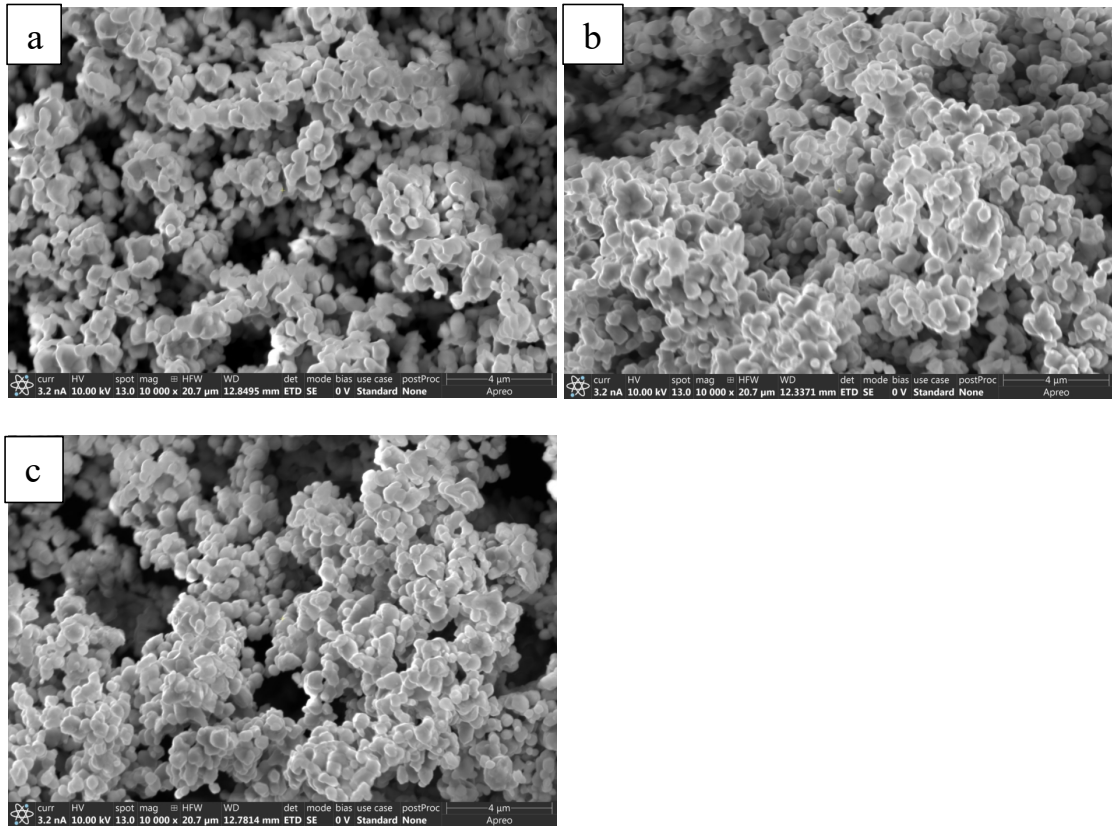
Fig. 15 SEM (10000×) pictures of sample 06 (a), 07 (b), 08 (c)

We performed SEM analysis to observe the morphology of cobalt ferrites we obtained, as shown in **Figure 15**. It can be easily observed that after annealing larger grain size was achieved due to growth behaviour at high temperature. This increase are positive correlated with annealing time.
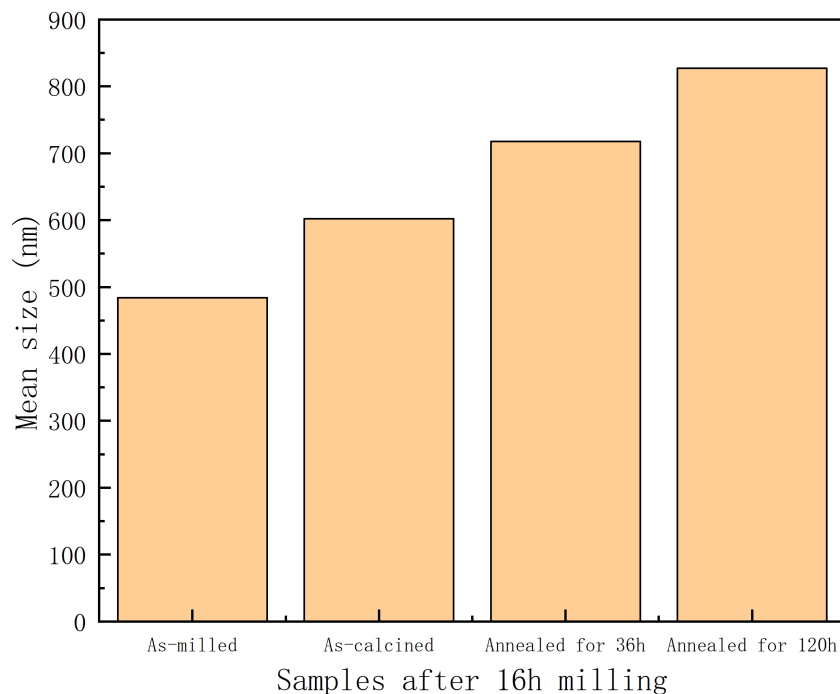
Fig. 16 Mean particle size of sample 05, 06, 07 and 08 (from left to right)

Besides, we performed DLS analysis as well to verify the consistence of the conclusion obtained from SEM result, and the result is demonstrated in **Figure 16**. Similarly, we can also get the conclusion that with increasing annealing time, particle size became larger, mainly because of growth during such process, consistent to the SEM result. During DLS test, we found that the solubility of cobalt ferrites to ethanol significantly decreased and aggregation occurred after annealing process. Since our cobalt ferrite nanoparticle was formed via high-energy ball milling, thereby it owns high surface energy, making it easier to aggregate to reduce the energy in order to keep system stable.
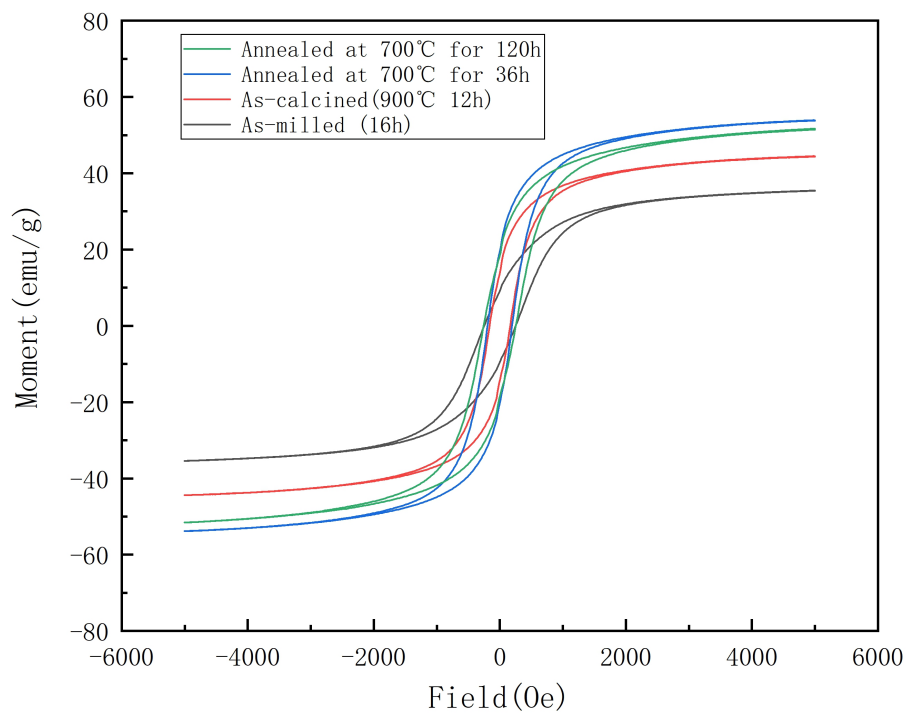
Fig. 17 Hysteresis loops of sample 05, 06, 07 and 08
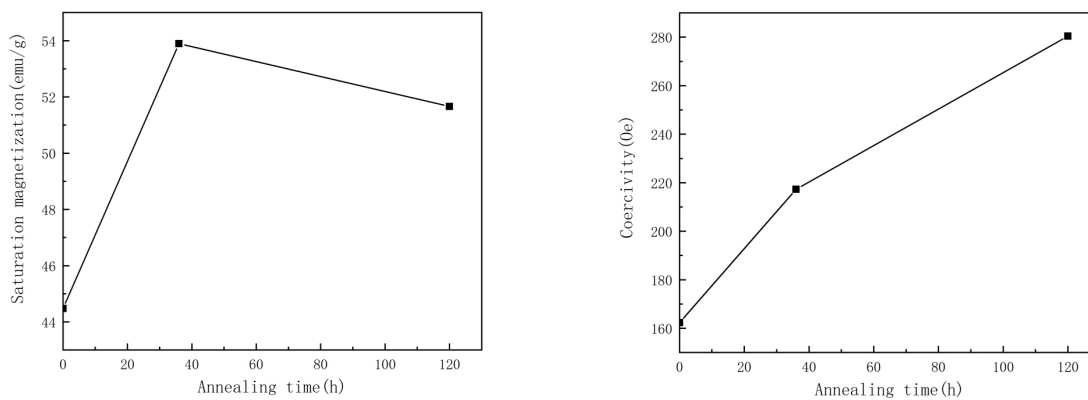
Fig. 18 Saturation magnetization and coercivity vs. Annealing time

Figure 17 shows hysteresis loops of sample 05, 06, 07 and 08, and **Figure 18** illustrates saturation magnetization and coercivity's relation with annealing time, tested by VSM at room temperature(300K). As-milled powder shows low saturation magnetization and high coercivity, and after calcination at 900 °C where single phase structure was formed, cobalt ferrite achieved high saturation magnetization and low coercive field, shows totally soft magnetic features, and such result is consistent with sample 01 and 03 mentioned in last section. After being annealed at 700 °C for 36h, we observed a big increase in saturation magnetization and coercivity. As we discussed in last section, larger grain size obtained from growth behaviour during annealing can make it easier for domain wall motion since the number of domains increased and grain boundary was diminished. Apart from influence of grain size, phase separation contributed a lot to the increase of M_s and coercive field. Single phase decomposed into iron-rich phase and cobalt-rich phase during annealing, increasing magnetic anisotropy which mainly resulted in higher coercivity. According to phase diagram of Fe-Co-O, as shown in **Figure 10**, estimated composition of iron-rich phase is $Co_{1.12}Fe_{1.84}O_4$, and composition of cobalt-rich phase is $Co_{2.69}Fe_{0.31}O_4$. Based on $M_s = |M_A-M_B|$ (the absolute value of the difference between A site and B site) and distribution of cations, we can evaluate M_s of iron-rich phase and cobalt-rich phase separately. It turns out that in composition $Co_{1.7}Fe_{1.3}O_4$, the combination of iron-rich phase and cobalt-rich phase owns higher saturation magnetization than single phase spinel structure. In a word, phase separation during annealing process at 700 °C for 36h shows positive influence on magnetic properties of cobalt ferrite. Coercivity still increased with a slower speed after being annealed at 700 °C for 120h. However, we observed that saturation magnetization slightly decreased when annealing time extended to 120h. Some explanations make sense to figure out this phenomenon. The first one is that with annealing time got longer and longer, grown grain

squeezed pores inside ferrite which may come from air and those pores remained in between boundaries, thereby domain wall motion was restricted. Another possible reason is small amount of antiferromagnetic Fe_2O_3 was precipitated during long time annealing, resulting in reduced Fe^{3+} cations and increased bivalent ions inside cobalt ferrite, consequently saturation magnetization decreased.

4.1.3 Milling Time

Sample 01, 05 and 09 are as-milled powder with different milling time, and sample 04, 07 and 11 are as-annealed powder (700 °C, 36h) based on sample 01, 05 and 09, separately. These two groups of samples were prepared to study how different milling time influenced properties and phase decomposition behaviour of cobalt ferrite.
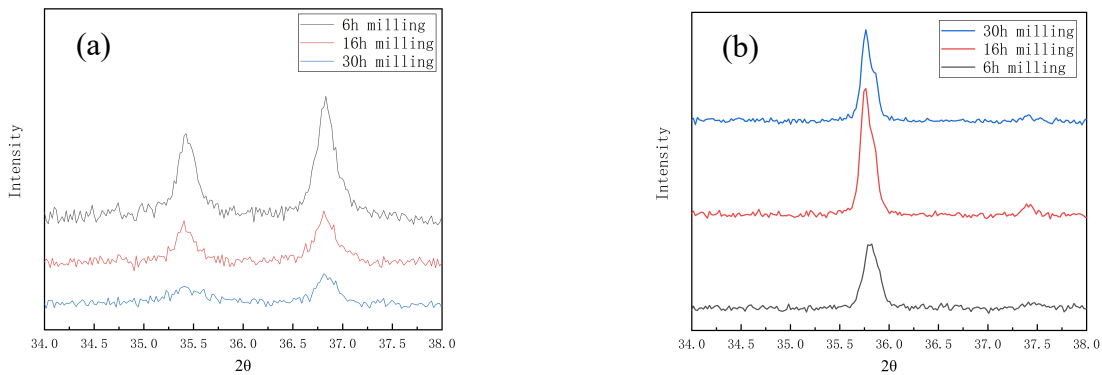
Fig. 19 XRD result of sample (a) 01, 05 and 09; (b) 04, 07 and 11

48

Figure 19 shows XRD result of these two group of samples. In **Figure 19(a)**, peak position of three as-milled powder are almost the same, indicating that no new main phase showed up after simply milling process. It's obviously with milling time decreased, peaks of Co_3O_4 and Fe_3O_4 which are our raw materials, became sharper. That implies the degree of mixing is positively correlated with milling time. The same conclusion could be found in **Figure 19(b)**. Secondary peak around 37.5° seems sharp in sample 07 and sample 11, furthermore, peak split took place in sample 11. However, in sample 04, secondary peak around 37.5° looks flat. This phenomenon could be explained by difference in mixing degree due to different milling time. In addition, main peak of sample 07 and 11 shows a slight left shift, indicating that phase separation took place. It is well known that high-energy ball milling could form numerous defects inside powder, which contributes to diffusion behaviour. Combined with the XRD result, we can conclude that long time ball milling could help promote phase decomposition during annealing process.
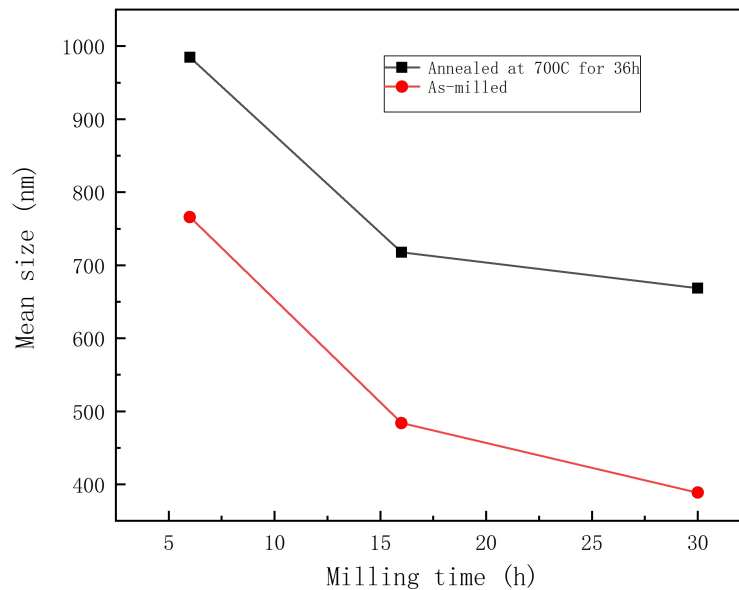
Fig. 20 Mean particle size of as-milled sample 01, 05 and 09 (red line), and as-annealed sample 04, 07 and 11 (black line) vs. miling time

We also performed DLS analysis to study influence of milling time on particle size, and the result is displayed in **Figure 20**. With milling time increased, particle size of as-milled powder got smaller, and so did the as-annealed samples. This result can be easily understood since the longer milling time is, the more crush and collide will be performed, thereby the particle size will decrease. Besides, we observed that the tendency of size decrease slowed down when milling time continued to extend. There is a limitation of size decrease in ball milling--we cannot keep refining the particle by performing high-energy ball milling. That is because with particle becomes finer, its surface energy will keep increasing, when the size scale reaches a very small level (like nano-particle), aggregation takes place to reduce energy in order to keep system stable. When we performed DLS analysis, we found aggregation was much easier formed in samples with long milling time, which is consistent with our conclusion above. Besides, after

being annealed, we observed increased size in all three samples, which is also same as what we discussed in last two sections.
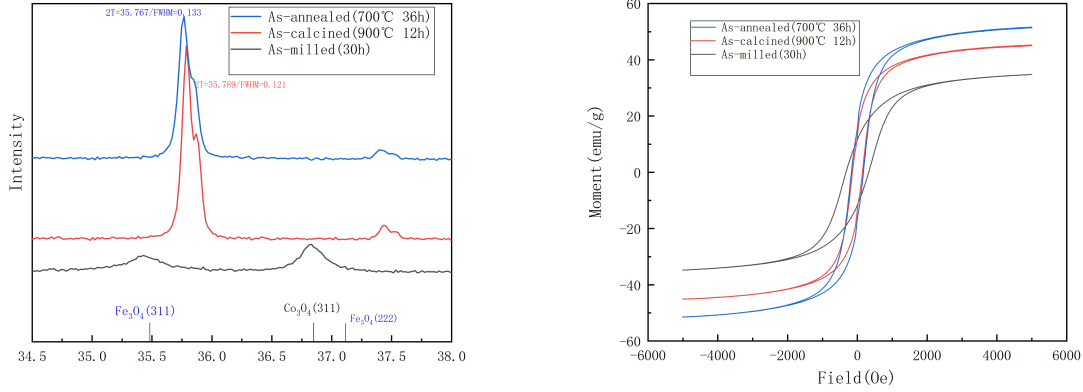
Fig. 21 XRD result and hysteresis loops of sample 09 (black), 10 (red) and 11 (blue)

Before we discuss how milling time influence magnetic properties of as-annealed sample 04, 07 and 11, we'd better show some properties of sample 09, 10 and 11 first, which all experienced ball milling for 30h. Sample 09 is as-milled, and sample 10 experienced calcination at 900 ℃ for 12h after milling. **Figure 21** illustrates XRD result and hysteresis loops of these samples. It is clearly that a slight left-shift and broadening of main peak in XRD pattern took place. After calcination at 900 ℃, single phase was formed and high saturation magnetization and low coercive field were obtained. After being annealed at 700 ℃ for 36h, both M_s and coercivity increased, which resulted from phase decomposition and larger grain size. However, magnitude of the increase was smaller than as-annealed sample 07, which was under ball milling for 16h.
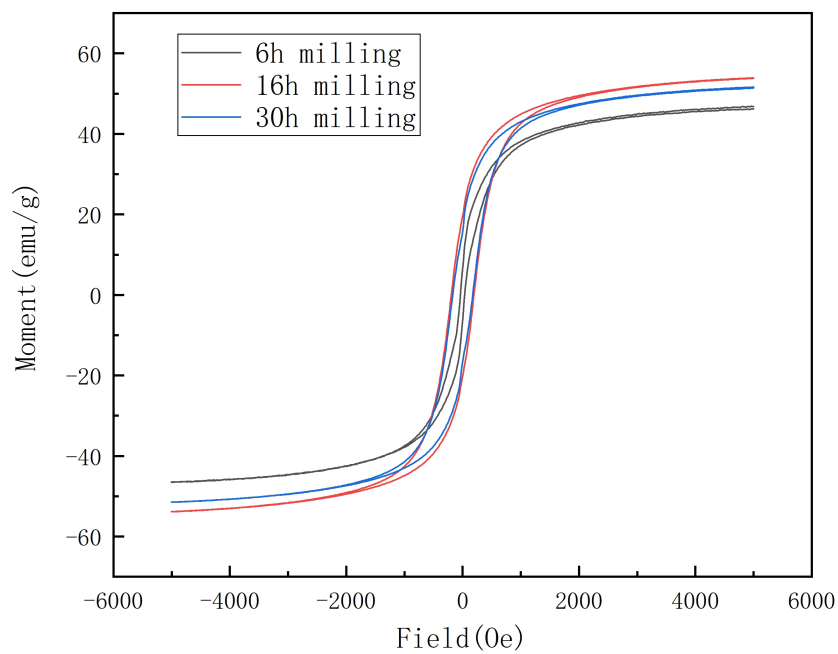
Fig. 22 Hysteresis loops of sample 04, 07 and 11 (as-annealed)
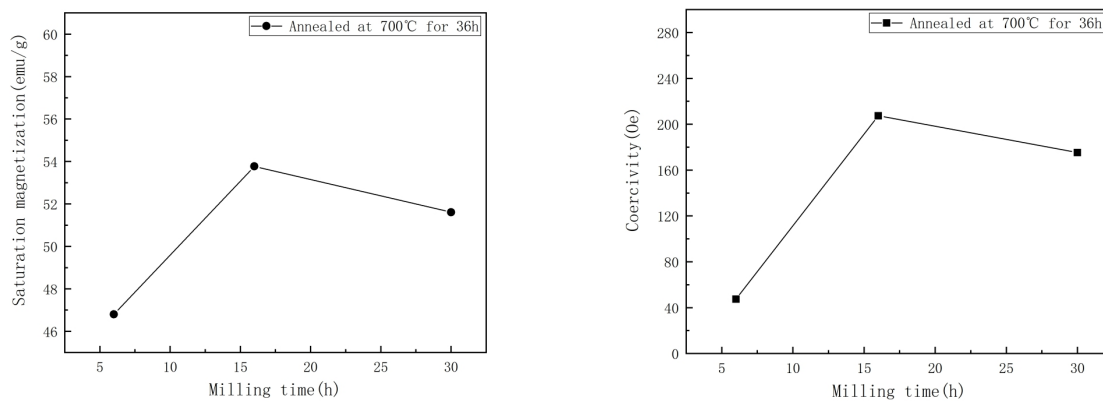
Fig. 23 Saturation magnetization and coercivity of as-annealed sample 04, 07 and 11 vs. Milling time

Hysteresis loops of sample 04, 07 and 11 are shown in **Figure 22**, and their saturation magnetization along with coercivity is displayed in **Figure 23**. Obviously, sample 04, which experienced milling for 6h, showed lowest coercivity and M_s. It is mainly because 6h is not long enough to form great mixture of two raw materials and defects to promote diffusion, which will help phase decomposed. When milling time increased to 16h, saturation magnetization and coercive field reached highest value, and after 30h milling, M_s and coercive field slightly decreased. The decrease of M_s might result from much more defects formed during 30h milling, which restricted domain wall motion. The decrease of coercivity might be related to diminished phase decomposition due to aggregation behaviour, which is easier to occur in powder which experienced longer milling.

4.1.4 Fe-Co Ratio

Samples (sample 01-11) we discussed above owns composition near left spinodal curve boundary. To further study the behaviour and properties of ferrites with composition near spinodal curve boundary, we made sample 21, 22 and 23, which are located near right boundary. We can compared these samples with sample 05, 06 and 07 to study how ratio made a difference and similarity between cobalt ferrite with different composition near spinodal curve boundary.
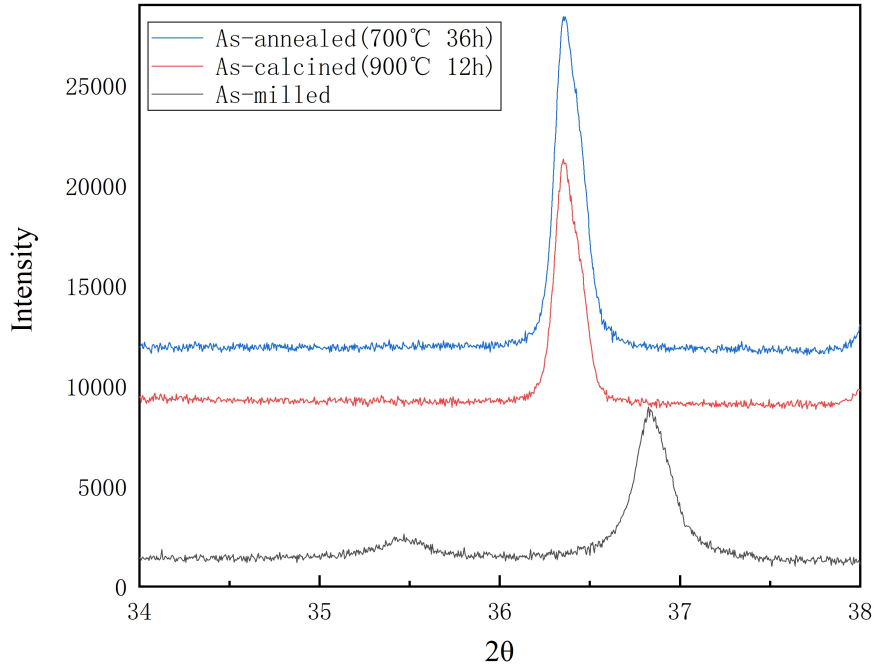
Fig. 24 XRD result of sample 21 (as-milled), 22 (as-calcined) and 23 (as-annealed)

Figure 24 shows XRD result of sample 21, 22 and 23. Same as previous samples, single phase was formed after calcination at 900℃. Since the content of cobalt increased significantly, peaks of cobalt ferrite had a huge right-shift. After anneal at 700℃ for 36h, neither peak splitting nor broadening was found, indicating that spinodal decomposition hardly occurred. Besides, a small peak appeared around 37.4° in sample 23, which may be viewed as cobalt-rich phase, implying that binodal decomposition played its part, the same as sample 07. These information obtained from XRD illustrates a similarity of phase decomposition behavior between cobalt ferrites located near spinodal curve boundary.

(a)

(b)
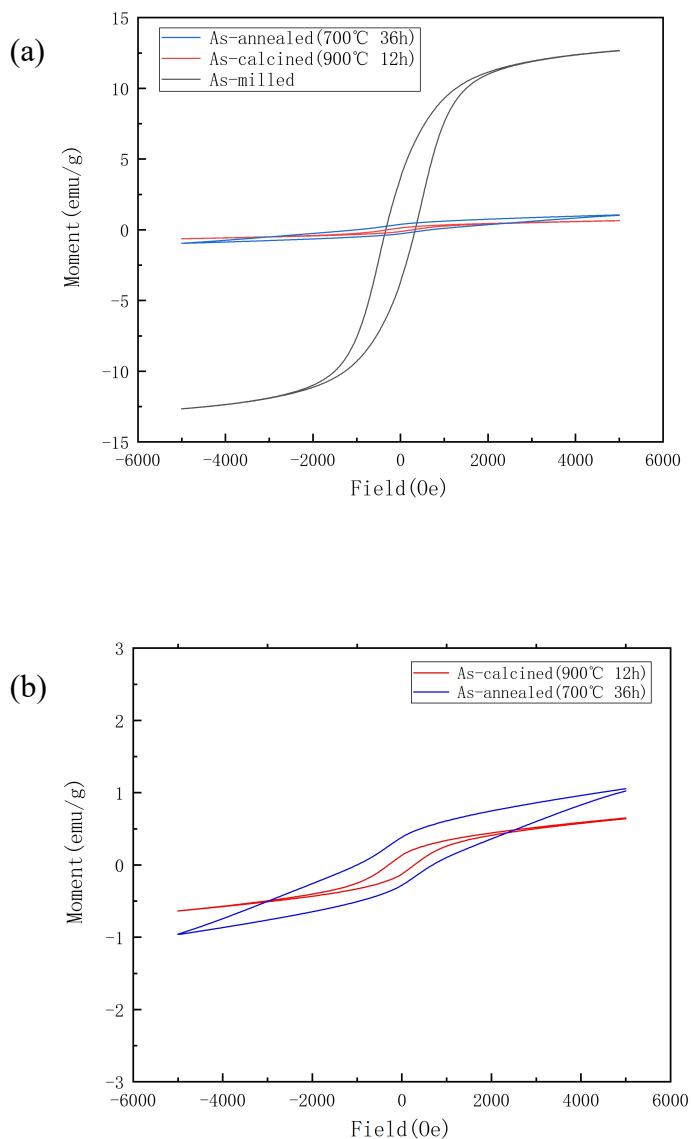
Fig. 25 Hysteresis loops of (a) sample 21, 22 and 23; (b) sample 22 and 23 enlarged view

In **Figure 25**, we can see the hysteresis loops of sample 21, 22 and 23 achieved from VSM. Sample 22, which is as-calcined powder, showed very low saturation magnetization closed to 0. After anneal, M_s slightly increased while coercivity had a huge increase. Low saturation magnetization can be attributed to high content of cobalt which made the ferrite show

55

similar behaviour to antiferromagnetic materials. High coercivity may result from formation of Fe-rich phase with high anisotropy and pinning effect of cobalt-rich phase during phase decomposition.

4.1.5 Brief Summary

In **chapter 4.1**, we discussed phase separation behavior, influences of different conditions and magnetic properties based on cobalt ferrites whose compositions were near spinodal curve boundary. We found that binodal decomposition tends to take the lead in this area when we talk about phase separation.

Different conditions influenced our products to some extend. When we applied different calcination temperature, ferrite with single phase or multiple phases were formed depending on specific temperature. With anneal time increased, we first observed a rise in saturation magnetization, then a slight decrease when anneal time reached 120h. Meanwhile, coercivity kept increasing when anneal time prolonged, but we can observe such increase became gradual.

Particle size was highly affected by milling time. It was negatively correlated with milling time and we could estimate that there is a limitation for such size refinement via ball mill because of increasing surface energy. When milling time was prolonged from 6h to 16h, we can observe increase in both saturation magnetization and coercivity, and as milling time reached 30h, decrease was found in saturation magnetization and coercive field.

Cobalt ferrites with compsitions located near left and right spinodal curve boundary shared similar phase separation behavior, which is binodal decomposition. Their huge difference of saturation magnetization, in both as-calcined and as-annealed cases, can be attributed to different cobalt content.

4.2 Composition In Center of Spinodal Area

In last section, we discussed on cobalt ferrites with composition near boundary of spinodal curve. In order to have the composition located near center part of spinodal area, we increased Co-Fe ratio by adding more Co_3O_4 before high-energy ball mill. Samples from 12 to 20, whose conditions in detail are shown in **Table 1**, were made based on this purpose. It is important to note that in this chapter, all compositions written down take iron solved during ball mill into consideration.
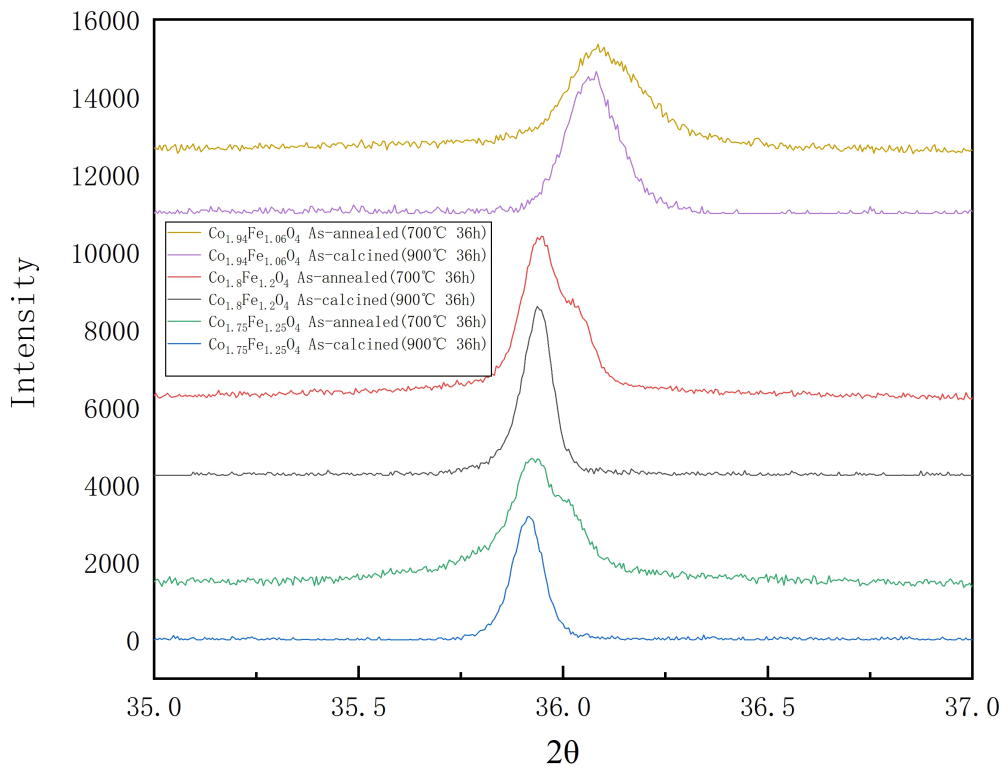
Fig. 26 XRD result of sample 16, 17, 13, 14, 19 and 20 (from bottom to top)

Figure 26 shows XRD result of as-calcined and as-annealed samples with 3 different compositions located in center part of spinodal area. Positions of peaks are different because of cobalt content--the more cobalt the ferrite owns, its peaks will shift more to right. We observed that after anneal process, significant peak broadening occurred in all three groups of samples, indicating the presence of spinodal decomposition, which is different from what we learned from previous samples referred in **chapter 4.1**. It proves that phase separation behaviour is highly related to composition.
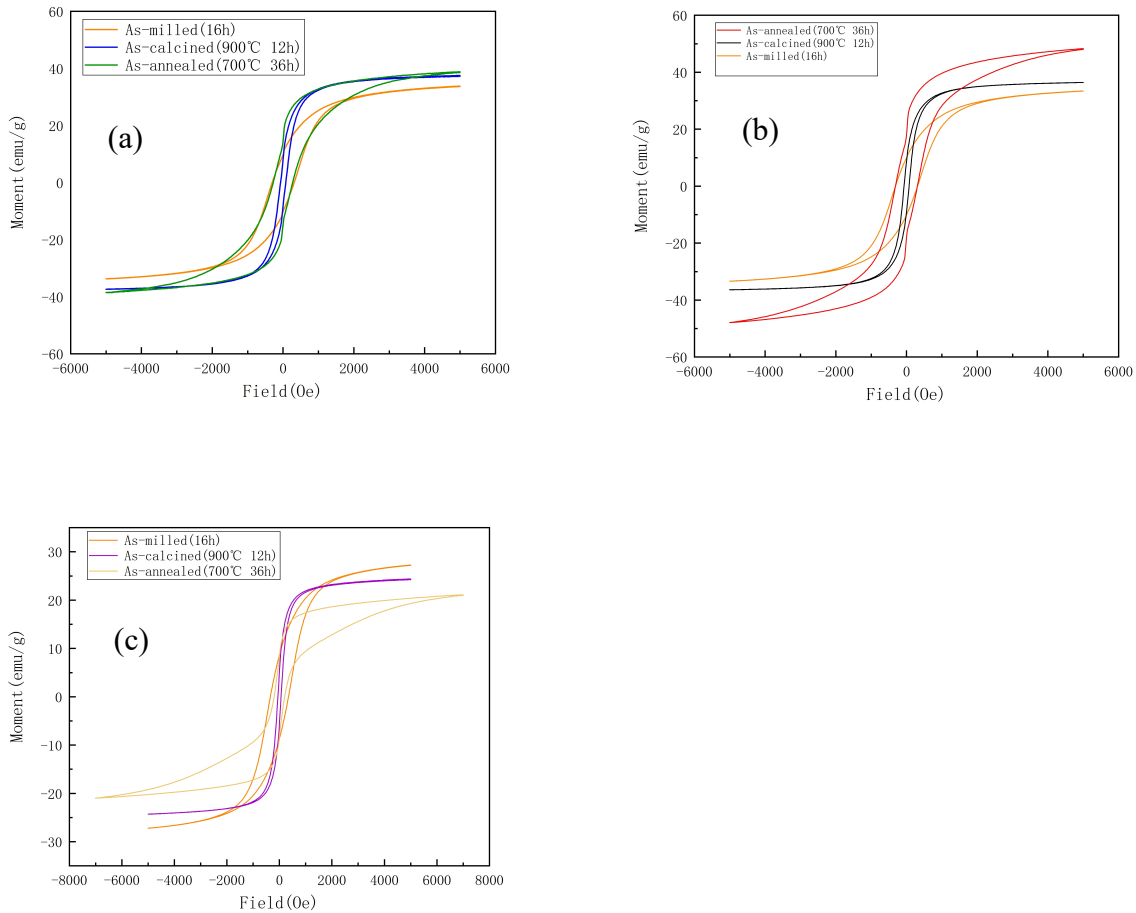
Fig. 27 hysteresis loops of (a) sample 15, 16 and 17; (b) sample 12, 13 and 14; (c) sample 18, 19 and 20

Hysteresis loops of such three groups of samples are revealed in **Figure 27**. **Figure 27(a)** is based on $Co_{1.75}Fe_{1.25}O_4$. Saturation magnetization got higher after calcination and anneal process, while coercivity decreased after calcination and increased after anneal. The same phenomenon can be found in **Figure 27(b)** as well, which is based on $Co_{1.8}Fe_{1.2}O_4$. Higher Ms resulted from formation of high saturation Fe-rich phase during spinodal decomposition, and increasing coercivity may be attributed to Co-rich phase as pinning points of domain wall motion, and high crystal anisotropy of Fe-rich phase. Different phenomenon appeared in **Figure 27(c)**, which is based on $Co_{1.94}Fe_{1.06}O_4$. Coercivity decreased after calcination and increased after anneal, same as the other two groups, but saturation magnetization declined. That can be explained by excess cobalt content. It is known that overall M_s is determined by sum of M_s of Co-rich phase, which is low, and Fe-rich phase, which is relatively high. When increasing cobalt content reached and then exceeded critical value, low M_s Co-rich phase will be more dominant and overall saturation magnetization showed a trend to decline.
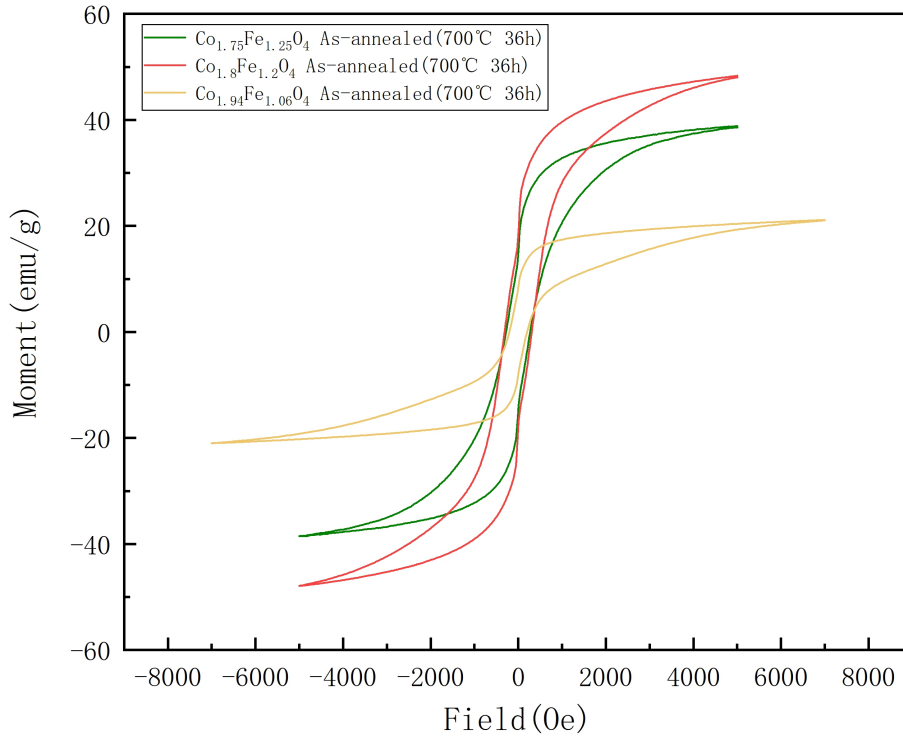
Fig. 28 hysteresis loops of as-annealed samples (sample 14, 17 and 20)

Besides, a special shape of hysteresis loops appeared after anneal in all the three groups, which is called wasp-waisted hysteresis loop. To reveal these loops more clearly, we put them together in **Figure 28**. We can clearly see that this shape owns a 'thin body' in low field. Such wasp-waisted hysteresis loop will show up if two phases mixed together and their coercivity are significantly different. Spinodal decomposition, different from binodal decomposition, is coherent phase separation and it involves a large scale all over the volume, and finally periodic structure is formed. Therefore, distinction between Fe-rich phase and Co-rich phase is more clear and thereby wasp-waisted loop appeared in our case.

4.3 Chemical composition

Now we are going to briefly discuss how composition acted as a factor to influence magnetic properties of cobalt ferrites $Co_xFe_{3-x}O_4$.
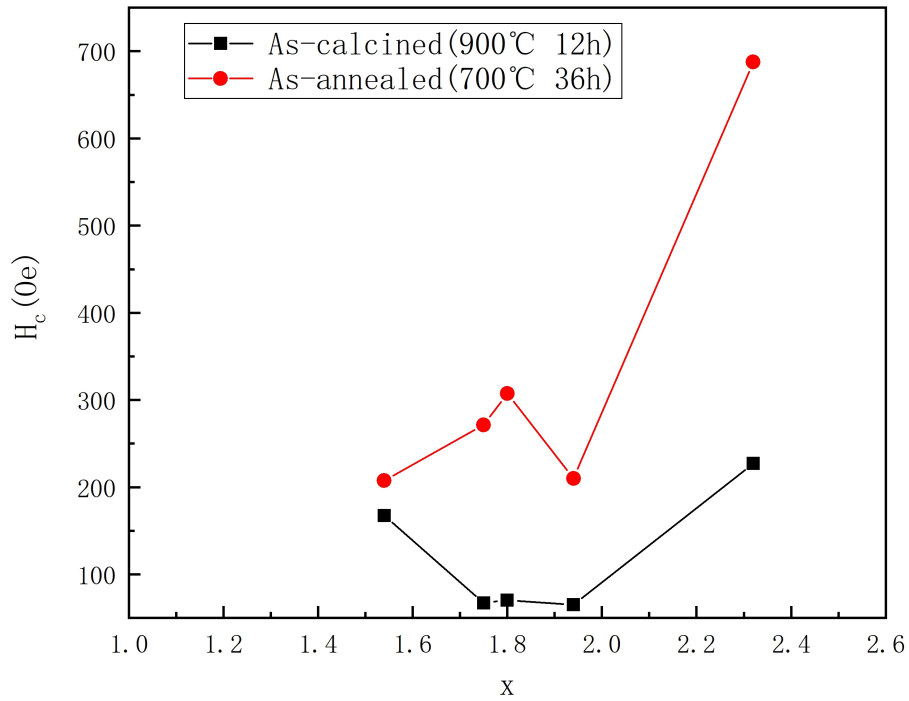
Fig. 29 Coercivity vs. Cobalt content fraction

Figure 29 shows correlation between coercivity and cobalt content fraction. When x located in center part of spinodal area, coercive field of as-calcined powders was pretty low, compared to ones near spinodal curve boundary. Coercivity increased after anneal process, or we can say after phase decomposition, in these samples, regardless of the value of x. It's hard to conclude that coercivity after anneal showed composition-dependence from our experiment.
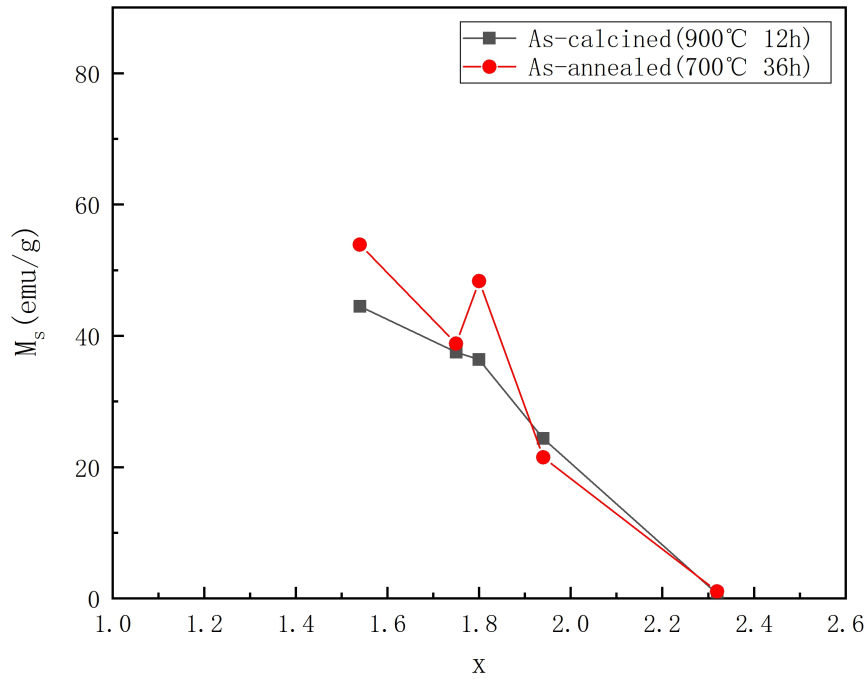
Fig. 30 Saturation magnetization vs. Cobalt content fraction

Figure 30 reveals correlation between saturation magnetization and cobalt content fraction. Ms of as-calcined powders showed clear composition-dependence--it decreased when more cobalt was added, which is well consistent with previous work run by Le Trong et al. [30], and in as-annealed powders almost the same tendency was founded. The unique red data point around x=1.8 may be attributed to measurement issue or specificity of the test subject.

5.0 Conclusion and prospect

Cobalt ferrites nanopowders($Co_xFe_{3-x}O_4$) were successfully made via high-energy planetary ball mill and subsequent calcination. After anneal, phase separation was observed. The phase separation behaviour and influence of different conditions, such as calcination temperature, annealing time, milling time, cobalt content fraction were characterized.

Saturation magnetization showed composition-dependence, to be more specific, negatively correlated to cobalt content fraction ($x \leq 2.34$), which is attributed to increase of antiferromagnetic cobalt ions. Coercive field did not show consistent composition-dependence.

Different phase separation behaviour was observed between samples with compositions located near spinodal curve boundary and ones around the center part of spinodal area. In former situation, binodal decomposition based on nucleation mechanism played the lead role, while spinodal decomposition dominated in latter situation. It may indicate that high-energy ball mill made a difference.

Proper calcination temperature is of vital for formation of single phase ferrites. Mixture of three phases appeared when the temperature was set at 700 °C, while single phase structure showed up as the temperature rose to 900 °C, consistent with how phase diagram revealed.

Annealing time played a important part in ferrites. Particle size got bigger with increasing annealing time, because of growth mechanism. Saturation magnetization increased in the early stage, which mainly resulted from Fe-rich phase with higher M_s formed during spinodal decomposition. With annealing time prolonged to 120h, saturation magnetization slightly decreased. It is likely that grown grain squeezed pores inside ferrite and those pores remained in between boundaries, thereby domain wall motion was restricted. Another possible reason is

63

small amount of antiferromagnetic Fe_2O_3 was precipitated during long time annealing, resulting in reduced Fe^{3+} cations and increased bivalent ions inside cobalt ferrite, consequently saturation magnetization decreased. Coercivity increased with annealing time, since Fe-rich phase with high crystal anisotropy and Co-rich phase acting as pinning point of domain wall motion were formed during phase separation. This means it is possible to control coercivity to some extent via anneal, which may help further optimize engineering.

Particle size was significantly influenced by milling time. It got smaller when more milling time was applied, and the refinement had a limitation. As-annealed sample under milling for 6h, showed lowest coercivity and M_s. It is mainly because 6h is not long enough to form great mixture of two raw materials and defects to promote diffusion. When milling time increased to 16h, saturation magnetization and coercive field reached highest value, and after 30h milling, M_s and coercive field slightly decreased. The decrease of M_s might be attributed to excess defects formed during 30h milling, which acted as pinning point restricting domain wall motion. The decrease of coercivity might be related to aggregation behaviour.

In our work, high-energy ball mill was proved to be a effective method to form spinel ferrite nanopowders. In further research, more samples based on different annealing time should be produced and tested to get more precise and consistent result. Besides, different annealing temperature is a good stand point. In addition to properties characterization, tests on performance are of vital, such as resistance test to see how periodic, incoherent phase mixture formed by spinodal decomposition performed differently from phase mixture formed by nucleation.

Bibliography

[1] A. Broese Van Groenou, P. F. Bongers, A. L. Stuyts. Magnetism, Microstrueture and Crystal Chemistry of Spinel Ferrites. Mater. Sci. Eng., 3 (1968/69) 317-392

[2] A. Goldman, Handbook of Modern Ferromagnetic Materials (Springer, Berlin, 1999)

[3] W. Kingery, H. Bowen, D. Uhlmann, Introduction to ceramics (John Wiley & Sons, New York, 1976)

[4] L. Neel, Magnetic properties of ferrites: ferrimagnetism and antiferromagnetism. Ann. Phys. 3, 137–198 (1948)

[5] J.S. Kim, W.H. Chang, The effect of calcining temperature on the magnetic properties of the ultra-fine NiCuZn-ferrites. Mater. Res. Bull. 44, 633–637 (2009)

[6] R.C. Pohanka, P.L. Smith, S.W. Freiman, L.M. Levinson, Electronic Ceramics, Properties, Devices and Applications. Recent Advances in Piezoelectric Ceramics, Electronic Ceramics (Marcel Dekker, New York, 1988)

[7] A. Goldman, Modern Ferrite Technology (Van Nostrand Reinhold, New York, 1990)

[8] C. Guillaud, The properties of manganese-zinc ferrites and the physical processes governing them. Proc. IEE-Part B Radio Electron. Eng. 104(5S), 165–173 (1957)

[9] T. Pannaparayil, R. Marande, S. Komarneni, Magnetic properties of high-density Mn–Zn ferrites. J. Appl. Phys. 69(8), 5349 (1991)

[10] J. Pankert, Influence of grain boundaries on complex permeability in MnZn ferrites. J. Magn. Magn. Mater. 138(1–2), 45–51 (1994)

[11] M.T. Johnson, E.G. Visser, A coherent model for the complex permeability in polycrystalline ferrites. IEEE Trans. Magn. 26(5), 1987–1989 (1990)

[12] A. Znidarsic, M. Drofenik, High-resistivity grain boundaries in CaO-doped MnZn ferrites for high-frequency power application. J. Am. Ceram. Soc. 82(2), 359–365 (1999)

[13] H. Shokrollahi, K. Janghorban, Influence of additives on the magnetic properties, microstructure and densification of Mn–Zn soft ferrites. Mater. Sci. Eng. B 141(3), 91–107 (2007)

[14] Abdollah Hajalilou, Saiful Amri Mazlan, A review on preparation techniques for synthesis of nanocrystalline soft magnetic ferrites and investigation on the effects of microstructure features on magnetic properties. Appl. Phys. A (2016) 122:680

[15] Tokatlidis S, Kogias G, Zaspalis VT. Low loss MnZn ferrites for applications in the frequency region of 1–3 MHz. J Magn Magn Mater 2018;465:727–35.

[16] Kalarus J, Kogias G, Holz D, Zaspalis VT. High permeability–high frequency stable MnZn ferrites. J Magn Magn Mater 2012;324:2788–94.

[17] Gheisari Kh, Javadpour S, Shokrollahi H, Hashemi B. Magnetic losses of the soft magnetic composites consisting of iron and Ni–Zn ferrite. J Magn Magn Mater 2008;320:1544–8.

[18] Rashidi S, Ataie A. Structural and magnetic characteristics of PVA/CoFe$_2$O$_4$ nano-composites prepared via mechanical alloying method. Mater Res Bull 2016;80:321–8.

[19] Moustafa SF, Morsi MB. The formation of Mg ferrite by mechanical alloying and sintering. Mater Lett 1998;34:241–7.

[20] Panneer Muthuselvam I, Bhowmik RN. Mechanical alloyed Ho^{3+} doping in CoFe$_2$O$_4$ spinel ferrite and understanding of magnetic nanodomains. J Magn Magn Mater 2010;322:767–76.

[21] Ding J, McCormick PG, Street R. Formation of spinel Mn-ferrite during mechanical alloying. J Magn Magn Mater 1997;171:309–14.

[22] Koohkan R, Sharafi S, Shokrollahi H, Janghorban K. Preparation of nanocrystalline Fe–Ni powders by mechanical alloying used in soft magnetic composites. J Magn Magn Mater 2008;320:1089–94.

[23] S. Zahi, M. Hashim, A.R. Daud, Synthesis, Magnetic properties and microstructure of Ni–Zn ferrite by sol–gel technique. J. Magn. Magn. Mater. 308(2), 177–182 (2007)

[24] M. Atif, M. Nadeem, R. Grossinger, R.S. Turtelli, Studies on the magnetic, magnetostrictive and electrical properties of sol–gel synthesized Zn doped nickel ferrite. J. Alloys Compd. 509(18), 5720–5724 (2011)

[25] C.F. Zhang, X.C. Zhong, H.Y. Yu, Z.W. Liu, D.C. Zeng, Effects of cobalt doping on the microstructure and magnetic properties of Mn–Zn ferrites prepared by the co-precipitation method. Phys. B Condens. Matter 404(16), 2327–2331 (2009)

[26] I. Sharifi, H. Shokrollahi, M.M. Doroodmand, R. Safi, Magnetic and structural studies on CoFe$_2$O$_4$ nanoparticles synthesized by co-precipitation, normal micelles and reverse micelles methods. J. Magn. Magn. Mater. 324(10), 1854–1861 (2012)

[27] T. Jahanbin, M. Hashim, K. Amin Mantori, Comparative studies on the structure and electromagnetic properties of Ni–Zn ferrites prepared via co-precipitation and conventional ceramic processing routes. J. Magn. Magn. Mater. 322(18), 2684–2689 (2010)

[28] S. Lomaev, L. Vasil'ev, Thermodynamically stable compositional inhomogeneous zones in the process of spinodal decomposition. Eur. Phys. J. Special Topics 229, 295-304 (2020)

[29] TAKAHASHI M, GUIMARÃES JRC, FINE ME. Spinodal Decomposition in the System $CoFe_2O_4$-Co_3O_4. J Am Ceram Soc 1971;54:291–5.

[30] Le Trong H, Barnabé A, Presmanes L, Tailhades P. Phase decomposition study in $Co_xFe_{3-x}O_4$ iron cobaltites: Synthesis and structural characterization of the spinodal transformation. Solid State Sci 2008;10:550–6.

[31] Le Trong H, Presmanes L, De Grave E, Barnabé A, Bonningue C, Tailhades P. Mössbauer characterisations and magnetic properties of iron cobaltites $Co_xFe_{3-x}O_4$ ($1 \leq x \leq 2.46$) before and after spinodal decomposition. J Magn Magn Mater 2013;334:66–73.

[32] S. Zahi, A.R. Daud, M. Hashim, A comparative study of nickel–zinc ferrites by sol–gel route and solid-state reaction. Mater. Chem. Phys. 106(2), 452–456 (2007)

[33] Syed Alamdar Hussain Shah, Vibrating Sample Magnetometery: Analysis and Construction, 2013

[34] A. Talaata, M.V. Suraj, K. Byerly, A. Wang, Y. Wang, J.K. Lee, P.R. Ohodnicki Jr, Review on soft magnetic metal and inorganic oxide nanocomposites for power applications. Journal of Alloys and Compounds 870 (2021) 159500